IMPURITY BAND CONDUCTION IN REDUCED SAMPLES OF BISMUTH IRON MOLYBDATE

by

SHAWN M. M^{c}INTYRE ©

A Thesis submitted in partial fulfillment
of the requirements of the Degree of
Master of Science

Department of Physics
Lakehead University
Thunder Bay, Ontario
Canada

June 14, 1995

ISBN 0-612-09223-2

ACKNOWLEDGEMENTS

It gives me great pleasure to thank Dr. W. M. Sears, my research supervisor, for his generous and instructive help throughout this thesis.

Special thanks to Dr. M. Hawton for her helpful insight into the topic of this thesis.

I wish to express my appreciation to Mr. G. C. Anderson for assisting in the construction and maintenance of the vacuum system and to Dr. V.V. Paranjape for his interest in the research topic.

I wish to thank Dr. W.J. Keeler for his generous offering of certain units used in constructing the vacuum system.

Finally, I wish to express my thanks to Ms. E.M. McDonald for typing my thesis.

ABSTRACT

An experimental investigation of the electrical resistance of n-type bismuth iron molybdate ($Bi_3FeMo_2O_{12}$) pellets at temperatures from 90 to 620 K has been made in an attempt to detect impurity band conduction near room temperature. The pellets were chemically reduced by exposing them to 13.2% methanol vapour in a nitrogen carrier gas inside an oven at 620 K. Lightly reduced samples yield an activation energy of 360 meV over the temperature region of 300 - 620 K which represents the donor energy level below the conduction band edge. A change in this activation energy over the temperature region of 150 to 300 K suggests the adsorption of water vapour or oxygen which tends to trap out carriers and suppress the pellet's conductance. For the more heavily reduced samples a near temperature independent resistance, in the temperature range of 90 to 300 K, suggests a metallic like conduction through an impurity band. A lowering of the activation energy, with increasing reduction, from 16 meV down to 1 meV suggests a transition from hopping to metallic conduction in the impurity band formed by the oxygen vacancy donor states. As the oxygen vacancy donor concentration increases the temperature region dominated by conduction through the impurity band expands to higher temperature. X-ray powder diffraction measurements reveal the formation of Bi, Bi_2O_3 or MoO_3 as well as MoO_2 during the reduction sequence, but have been excluded as an explanation of the metallic like behavior observed in the temperature region of 90 to 300 K due to the small amounts observed.

TABLE OF CONTENTS

Page

LIST OF FIGURES

LIST OF TABLES

INTRODUCTION

It was postulated by C.S. Hung[1,2] that impurity band conduction (i.e., electrical conduction through a band of energy levels formed by the impurities) is characterized by a temperature independent resistance. This happens at some critical impurity concentration N_C. This temperature independence reflects a type of conduction where the electron orbiting about its impurity center moves freely from one impurity center to another through the strong overlapping of electron ground state wave functions. In practice conduction through this band of impurities is almost, but not quite, independent of temperature and is characterized by an activation energy of the order of 1 meV.

Mott[3] proposed that a transition to a state exhibiting metallic conduction occurs when the interatomic distance between impurities reaches some definite value. Above this distance a type of hopping or tunneling conduction can occur where the conduction is characterized by an activation energy of tens of meV.

Oxygen vacancies act as donor traps in $Bi_3FeMo_2O_{12}$. Thus as oxygen is removed, for example by methanol vapour at 620 K, $Bi_3FeMo_2O_{12}$ transforms into an n-type semiconductor material with the conductance increasing as the concentration of oxygen vacancies increase. Morrison [4,5] observed in a similiar material, bismuth molybdate, that oxygen vacancies formed by the reduction process produced donor levels within the forbidden band gap of 2.8 eV[6] at about 0.35 eV below the conduction band edge. He suggested that increasing levels of conductance signified the presence of higher concentrations of oxygen donor vacancies.

Other sources in the catalytic literature [4,5,7,8] specify that it is possible to remove 0.05% of the oxygen in bismuth molybdate and still retain crystallographic stability. This represents about 10^{19} vacancies per cubic centimeter. In a pure methanol atmosphere it is, in fact, possible to remove 1.0% of the oxygen to produce 10^{20} vacancies per cubic centimeter and still retain crystal stability.

Since it is proposed in this thesis that the oxygen vacancy donors lie 0.36 eV below the conduction band edge of $Bi_3FeMo_2O_{12}$ metallic like conduction via the impurity band may dominate even near room temperature.

This thesis is about a search for supporting evidence for impurity band conduction in n-type bismuth iron molybdate ($Bi_3FeMo_2O_{12}$) in the temperature region of 90 to 300 K.

CHAPTER 1

THEORETICAL BACKGROUND

1.1 Intrinsic Semiconductor

Intrinsic conductivity in semiconductors is a current carried by electrons and holes in the conduction and valence bands formed by the host atom. Room temperature resistivities of semiconductors are typically between 10^{-3} and 10^{9} ohm-cm compared to metals with typical values near 10^{-6} ohm-cm, and good insulators, with values as high as 10^{22} ohm-cm. Semiconductor band gaps range from about 3.0 eV down to a few tenths of an electron volt. It is suggested that an energy gap of 4.0 eV represents an arbitrary separation between semiconductors and insulators.[9]

The kind of energy band diagram generally used in semiconductor work is shown in Figure 1.1.1. Here only the bottom of the conduction band and top of the valence band are of interest. The electron energies of Figure 1.1.1 (a) are plotted against distance to show that there are no free carriers at T = 0 K. By elevating the temperature of the crystal lattice, thermal excitation will occasionally free an electron from the valence band creating a conduction electron and a hole as shown in (b). The simultaneous production of equal numbers of electrons and holes gives rise to an electrical conductivity that is in equilibrium with the continual process of thermal generation and recombination. The mass action law states that np = K where n is the electron concentration per unit volume, p is the hole concentration per unit volume and K is an equilibrium constant which is a function of temperature.

In a pure semiconductor, for every conduction electron produced a hole is also produced and n = p. Thus the total number of electrons or holes is called the intrinsic charge carrier concentration $n_i = n = p$. The intrinsic carrier concentration is then $n_i^2 = np$ because both the electrons in the conduction band and holes in the valence band contribute to the electrical conductivity.[10]

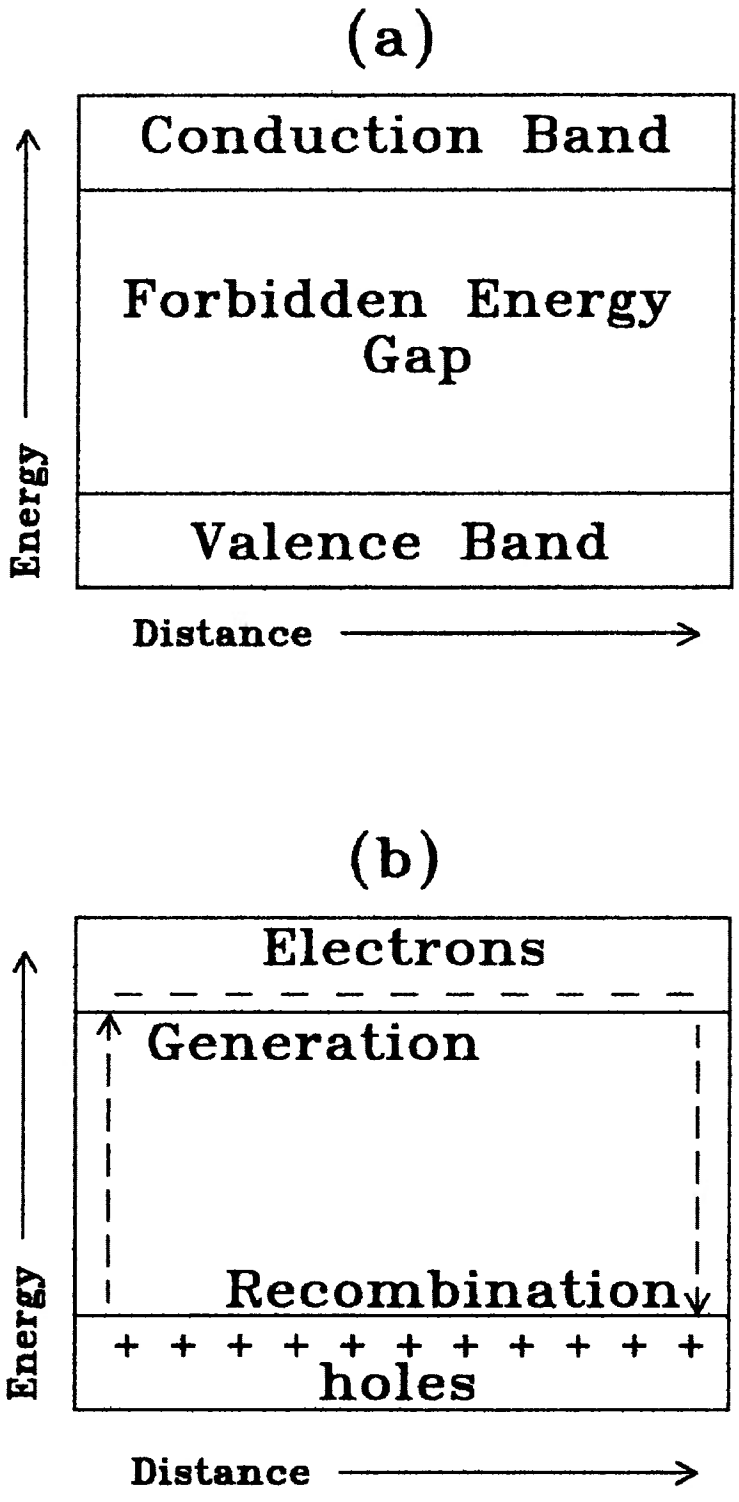

Figure 1.1.1 Intrinsic Semiconductor (a) at low temperature (b) at elevated temperature with thermal excitation generating holes and electrons

For the concentration of intrinsic carriers in terms of the band gap we assume simple parabolic band edges.[11,12,13,14] The number of occupied conduction band levels is given by

$$n = \int_{E_c}^{\infty} N_e(E)\, F_e(E)\, dE \qquad \text{eq'n 1.1.1}$$

where E_C is the energy at the bottom of the conduction band, $N_e(E)$ is the density of states and $F_e(E)$ is the Fermi Dirac distribution function.

The density of states can be approximated by

$$N_e(E) = \frac{1}{2\pi^2}\left(\frac{2m_e}{\hbar^2}\right)^{3/2}(E - E_C)^{1/2} \qquad \text{eq'n 1.1.2}$$

where m_e is the effective mass of the electron.

$F_e(E)$ can be approximated by the boltzmann distribution if $(E_C - E_F) >> kT$ and thus $F_e(E) << 1$. Thus

$$F_e(E) = \left[1 + \exp\frac{E - E_F}{K_B T}\right]^{-1} \cong \exp\left[\frac{E_F - E}{K_B T}\right] \qquad \text{eq'n 1.1.3}$$

where E_F is the fermi energy level.

Substituting equation 1.1.2 and 1.1.3 into equation 1.1.1 and integrating gives the concentration of intrinsic electrons in the conduction band.

$$n = 2\left(\frac{m_e K_B T}{2\pi\hbar^2}\right)^{3/2} \exp\left[(E_F - E_C)/K_B T\right] \qquad \text{eq'n 1.1.4}$$

For the equilibrium concentration of holes p, the distribution function for holes F_h is related to the electron distribution function F_e by $F_h = 1 - F_e$. Therefore

$$F_h(E) = 1 - \left[1 + \exp\left(\frac{E - E_F}{K_B T}\right)\right]^{-1} \cong \exp\left[(E - E_F)/K_B T\right] \qquad \text{eq'n 1.1.5}$$

provided that $(E_F - E_V) >> K_B T$.

The density of hole states is

$$N_h(E) = \frac{1}{2\pi^2}\left(\frac{2m_h}{\hbar^2}\right)^{3/2}(E_V - E)^{1/2} \qquad \text{eq'n 1.1.6}$$

where m_h equals the effective mass of the hole and E_V is the energy of the valence band edge. The concentration of holes p in the valence band would then be

$$p = 2\left(\frac{m_h K_B T}{2\pi\hbar^2}\right)^{3/2} \exp\left[(E_V - E_F)/K_B T\right] \qquad \text{eq'n 1.1.7}$$

Multiplying equations 1.1.4 and 1.1.7 and given the energy gap $E_g = E_C - E_V$, we obtain the intrinsic carrier concentration

$$n_i^2 = np = 4\left(\frac{K_B T}{2\pi\hbar^2}\right)^3 (m_e m_h)^{3/2} \exp\left(-E_g / K_B T\right) \qquad \text{eq'n 1.1.8}$$

The number of conduction electrons excited across the energy gap at temperature T is then

$$n_i = 2\left(\frac{K_B T}{2\pi\hbar^2}\right)^{3/2} (m_e m_h)^{3/4} \exp\left(-E_g / 2K_B T\right) \qquad \text{eq'n 1.1.9}$$

Since the current density $J = neV_D$ where V_D is the drift velocity, then the electrical conductivity $\sigma = J/E = nev_D/E = ne\mu_D$ where μ_D is the drift mobility. Introducing the mobility μ_e for electrons and μ_h for holes, the conductivity can be expressed as

$$\sigma = \left(ne\mu_e + pe\mu_h\right) \qquad \text{eq'n 1.1.10}$$

Substituting equation 1.1.9 into 1.1.10 we obtain

$$\sigma_i = 2e\left(\mu_e + \mu_h\right)\left(K_B / 2\pi\hbar^2\right)^{3/2} T^{3/2} (m_e m_h)^{3/4} \exp\left(-Eg / 2K_B T\right) \qquad \text{eq'n 1.1.11}$$

At room temperature the factor $\exp\left(-E_g / 2K_B T\right)$ is approximately 10^{-35} for $E_g = 4.0$ eV, but is $\approx 10^{-2}$ for $E_g = 0.25$ eV. Here we see that the conductivity depends critically on the size of the energy band gap[15]. The factor $T^{3/2}$ and the mobilities change slowly with temperature compared with the exponential term. The number of electrons thermally

excited into the conduction band must be a rapidly increasing function of temperature. The resistivity must therefore be a rapidly decreasing function of temperature.

1.2 Extrinsic Semiconductor (n-type)

Charge carriers in semiconductors can also be created by adding certain types of impurity atoms. If a group V element is added to a pure crystal of silicon, it occupies a lattice site that is normally occupied by the host atom. Four of the valence electrons of the impurity make covalent bonds with the host atom, but a fifth electron is bound to the impurity atom itself by a weak electrostatic force. This electron moves around the impurity site in a manner similar to an electron in a hydrogen atom. The electron is weakly bound to the impurity in the solid and may encompass hundreds of atomic lattice distances. However this level must lie below the lowest "free" electron state in the conduction band. Furthermore the binding energy of the electron to the donor impurity is small compared with the energy gap of the semiconductor and must therefore lie in the intrinsic energy gap. We conclude that donor impurities introduce additional electronic levels at energies E_D lower than E_C and lie close to the boundaries of the forbidden energy region. Therefore it is far easier to thermally excite an electron into the conduction band from a donor level than it is to excite an electron across the entire energy gap from valence to conduction band.[16, 17, 18]

The concentration of charge carriers in extrinsic semiconductors is illustrated in a graphical manner in Figure 1.2.1. In an extrinsic semiconductor the impurity curve is less steep because E_D is much smaller than E_g. As the temperature is increased, eventually the donor levels will be exhausted, meaning that all the donors have been ionized. An electron trapped in the donor state produces a neutral site whereas an electron excited into the conduction band leaves behind a positive donor site. In this region the conductivity becomes relatively independent of temperature. At a higher temperature intrinsic behavior becomes important.[19, 20]

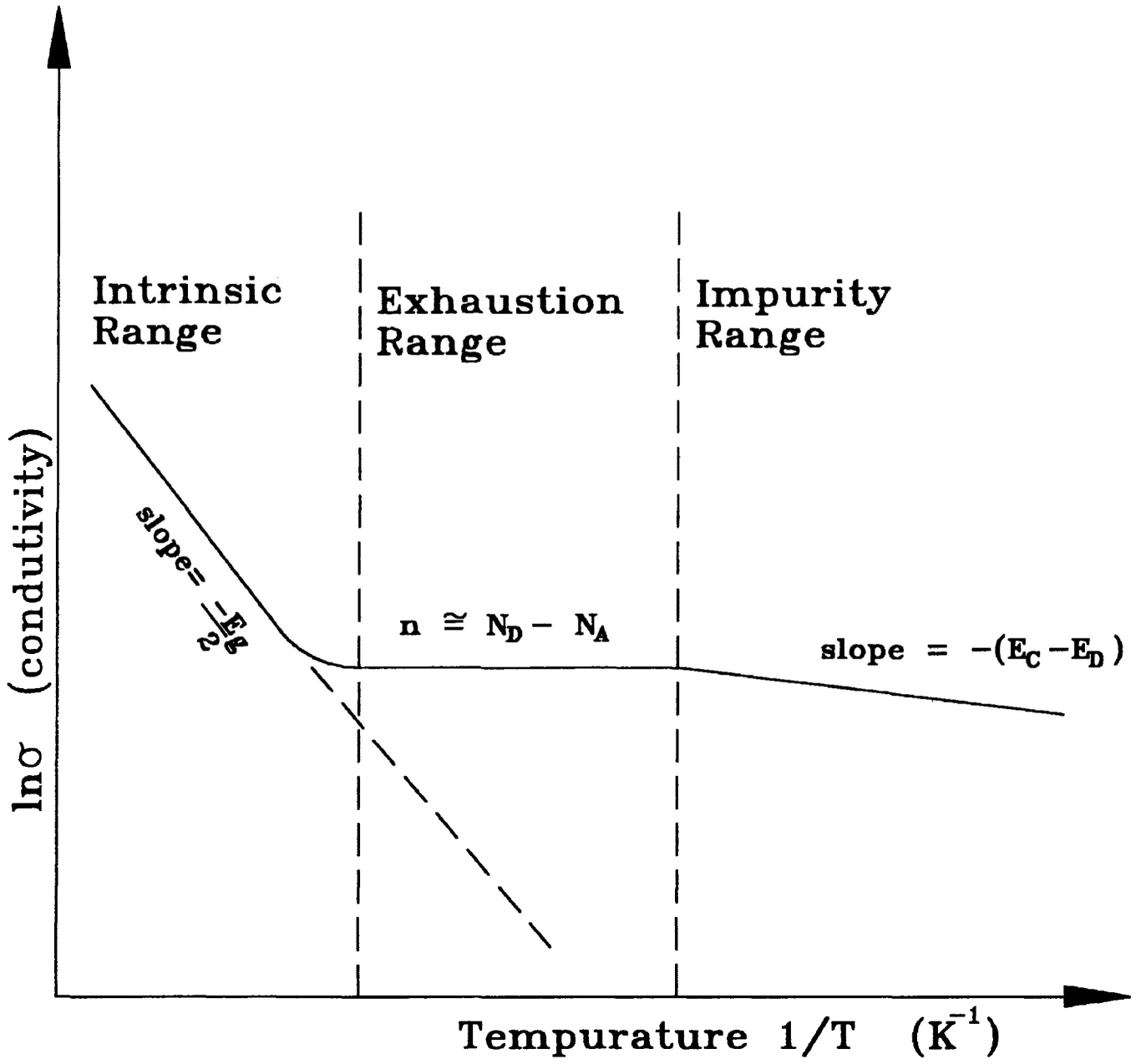

Figure 1.2.1 Conductivity as a function of temperature in an n-type (donor) extrinsic semiconductor

The distribution of electrons in all states can be described by a general set of equations as follows.[13, 21] The density of electrons in the conduction band (where N_C is the effective density of states in the conduction band) is given as:

$$n = N_C f_e(E_C) \qquad \text{eq'n 1.2.1}$$

The density of holes in the valence band (where N_V is the effective density of states in the valence band) is given as:

$$p = N_v\left[1 - f_h(E_v)\right] \qquad \text{eq'n 1.2.2}$$

The density of filled donor sites is expressed as

$$n_D = N_D f(E_D) \qquad \text{eq'n 1.2.3}$$

whereas the density of filled acceptors is given as

$$n_A = N_A f(E_A) \qquad \text{eq'n 1.2.4}$$

Finally the charge neutrality condition states that

$$p + (N_D - n_D) = n + (N_A - n_A) \qquad \text{eq'n 1.2.5}$$

where N_D and N_A are the densities of donor and acceptor centers. If we consider setting $N_A = 0$ then $p \cong 0$ and

$$n = N_D - n_D \qquad \text{eq'n 1.2.6}$$

which means that an n-type semiconductor supplies electrons from the donors to the conduction band. The number of electrons in the conduction band is given by equation 1.1.4 with $E_F = E_D$.

$$n = 2\left(\frac{2\pi m_e K_B T}{h^2}\right)^{3/4} \exp\left(\frac{E_D - E_C}{K_B T}\right) \qquad \text{eq'n 1.2.7}$$

Here we consider only partial ionization of donors at ordinary temperatures and low carrier concentration near the bottom of the conduction band where $n < N_D$ and $K_B T << E_C - E_D$.

1.3 Mobility

An electron subjected to an electric field in a solid is scattered by collisions with the fixed lattice. This results in a drift velocity. The drift mobility is defined as the magnitude of the drift velocity (cm/sec) per unit electric field (volt/cm)

$$\mu_D = \frac{|V_D|}{E} \qquad \text{eq'n 1.3.1}$$

The vibrations of an atom in a periodic lattice about an equilibrium position disturbs the periodicity and sets up local changes that scatter moving carriers (electrons and holes). As the temperature increases the amplitude of these lattice vibrations increase. Theoretically in the lattice-scattering range the mobility should follow the following temperature law[22]

$$\mu_L = B_1 T^{-3/2} \qquad \text{eq'n 1.3.2}$$

where B_1 is a constant of proportionality.

Ionized impurity scattering (coulomb scattering) deflects moving carriers near the location of the impurity ion. At high impurity concentrations or at low temperature impurity scattering dominates. The ionized impurity scattering limited mobility is given by the relation[22]

$$\mu_I = B_2 T^{3/2} \qquad \text{eq'n 1.3.3}$$

where B_2 is a constant of proportionality.

Combining equation 1.3.2 or 1.3.3 with equation 1.2.7 and 1.1.10 we will obtain a formula for the temperature dependence of the conductivity of electrons in the conduction band for n-type semiconductors.

$$\sigma_L = 2eB_1\left(\frac{2\pi m_e K_B}{h^2}\right)^{3/2} \exp\left(\frac{E_D - E_C}{K_B T}\right) \qquad \text{eq'n 1.3.4}$$

or

$$\sigma_I = 2eB_2\left(\frac{2\pi m_e K_B}{h^2}\right)^{3/2} T^3 \exp\left(\frac{E_D - E_C}{K_B T}\right) \qquad \text{eq'n 1.3.5}$$

depending on the type of electron scattering which dominates. Since σ_L and σ_I are in series for lattice and impurity ion scattering the σ's add as inverses (i.e., $1/\sigma_{total} = 1/\sigma_L + 1/\sigma_I$). Thus above 100 K and high impurity content σ_L will dominate.[23]

1.4 Theory of Impurity Band Conduction

For any partly filled band of a perfect crystal the material is a metal whose resistivity falls to zero as the temperature tends to zero. For a perfect crystal whose bands are either full or empty the crystal is a semiconductor whose resistivity tends to infinity as the temperature tends to zero. For an impurity doped semiconductor crystal the resistivity tends to a finite value.[24] The onset of this behavior shifts to higher temperatures with increasing concentrations of impurity atoms.

As an explanation C.S. Hung postulated the formation of a conducting impurity band within the forbidden band gap. It is here that a small but finite residual conductivity takes place in addition to conduction in the ordinary conduction band.[1, 2, 25]

Figure 1.4.1 illustrates the simple energy level diagram for an n-type impurity semiconductor containing $N_D > N_A$ concentrations of donors and acceptors respectively. Electricity can flow in an impurity doped semiconductor by two competing conduction processes which act in parallel. The first is a current carried by electrons in the conduction band or holes in the valence band. The second process is possible under certain circumstances. An electron occupying an isolated donor has a wave function localized about the impurity and an energy slightly below the conduction band minimum. A localized wave function is one that decays exponentially to zero at large distances from a given point in space. A conduction process is possible if there is a small but finite overlap

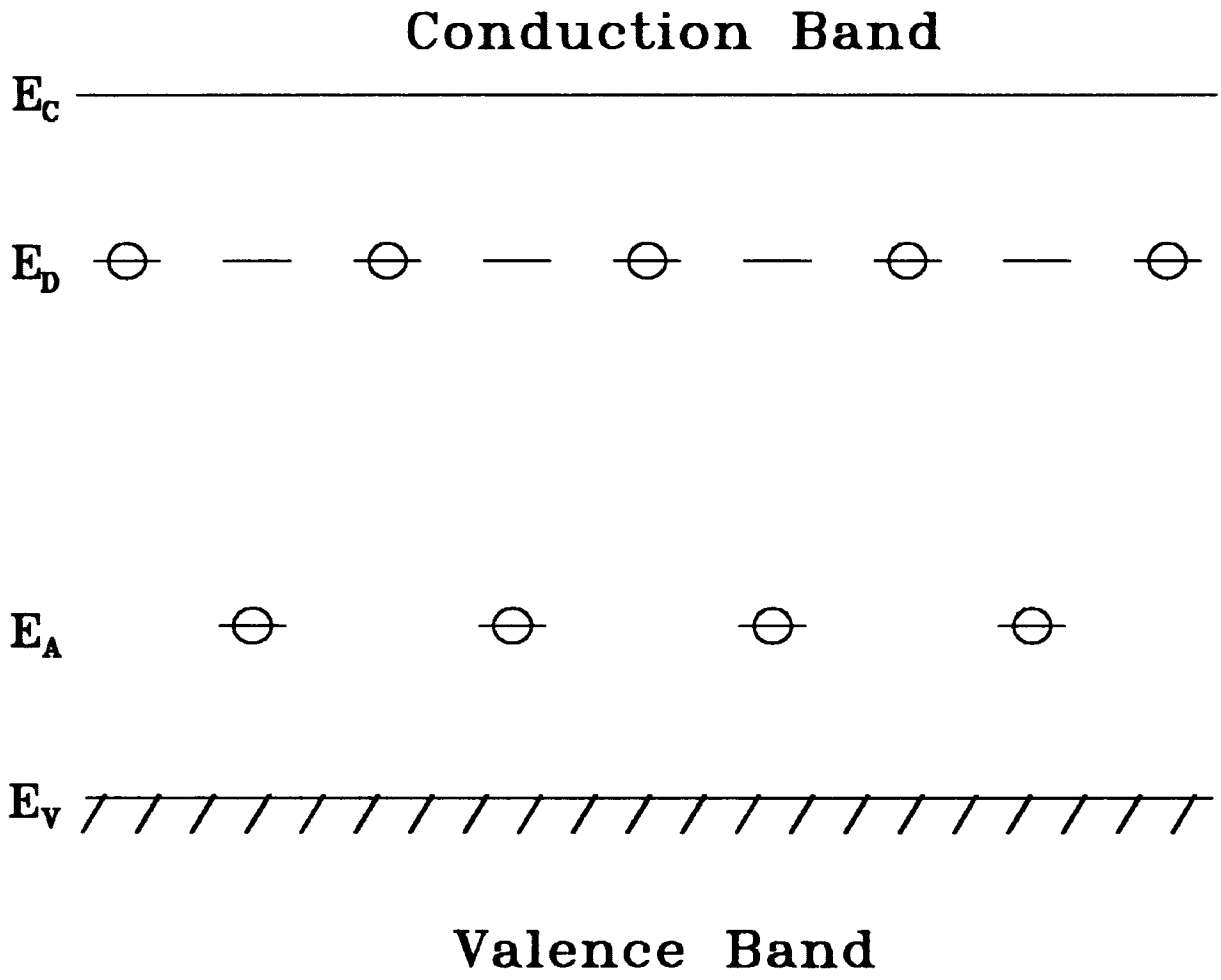

Figure 1.4.1

Schematic energy level diagram for an n-type impuity semiconductor containing $N_D > N_A$ concentrations.

of the wave function of an electron on one donor with that of a neighbouring unoccupied donor. At small impurity concentrations, impurity conduction is not possible unless compensating minority impurities are present. The occupied impurity centers, being separated by more than a few " radii " of the ground state wave function, require the presence of compensating minority impurities (e.g. acceptors in an n-type material) to produce unoccupied centers for transferring charge by tunneling or diffusion. Also when the impurity concentration is small, the finite activation energy suggests that charge transfer between impurity centers must itself be thermally activated. Thermal energy in the form of phonons is supplied by the vibrations of the host crystal.[26]

At donor impurity concentrations above a critical concentration N_C, the wave functions of individual adjacent impurities overlap strongly to sufficiently remove the localization of carriers about the impurity centers. The result is a temperature independent resistivity where the conductivity behaves as though it were metallic and carriers move freely without thermal activation. Although the mobility of electrons in the impurity levels is small, at low temperatures impurity conductivity will dominate due to the absence of electrons in the conduction band.[27] The term impurity conduction is used to describe the different types of conduction processes occurring in semiconductors for different values of impurity concentrations above and below the critical impurity concentration N_C. At low concentration there exists a hopping conduction. Above N_C there is a metallic like conduction through an impurity band.[28]

It has been ascertained experimentally that in the limit of low temperature the conductivity can be described by[29]

$$\sigma_{IBC} = \sigma_2 \exp(-\varepsilon_2 / K_B T) \qquad \text{eq'n 1.4.1}$$

The possibility for such a temperature dependence involves excited states higher in energy than the ground state in the impurity band. The extension of the excited electron wave function should have a considerably higher jump frequency than the electron in the ground state.

1.5 Hopping Conduction and the Transition to Metallic Conduction

In lightly doped semiconductors with an impurity concentration N_D, the average distance between impurities is greater than the Bohr radius a_H (i.e., $N_D^{-1/3} >> a_H$). In this case the necessary condition for hopping conduction is that the degree of compensation K be much less than one where $K = N_A/N_D$. $N_D - N_A$ donors are left to absorb phonons which cause the jump from occupied to unoccupied donor sites. This is the reason for the finite activation energy of hopping conduction.[30, 31]

In the case of heavily doped semiconductors satisfying the inequality $N_D^{-1/3} < a_H$, the average distance between impurities is less than the Bohr radius. The electrons form an almost perfect fermi gas and the conduction is metallic.[3]

The total conductivity of a lightly doped semiconductor is of the form[32]

$$\sigma = \sigma_1 \exp^{-\varepsilon_1 / K_B T} + \sigma_2 \exp^{-\varepsilon_2 / K_B T} \qquad \text{eq'n 1.5.1}$$

where the first term represents the contribution of the conduction through the conduction band and the second term the contribution of hopping conduction in the impurity band. At sufficiently low temperature the second term will dominate. The transition from hopping to metallic conduction is seen experimentally as a reduction in the activation energy of the second term. A near zero activation energy means metallic conduction.

The transition to a state of metallic conduction is expected to occur when the impurity concentration exceeds a critical value N_C. McIrvine (1960)[33] derived an empirical formula relating N_C to the dielectric constant (ε) and the Bohr radius (a_H).

$$N_C = (2.2\, a_H)^{-3} \exp(1 - \varepsilon) \qquad \text{eq'n 1.5.2}$$

1.6 Impurity Band Conduction in n-type Germanium and other n-type Semiconductors

A germanium crystal has an energy band gap of 0.67 eV at 300 K[34]. Germanium doped with low concentrations of antimony produces a donor level 0.0096 eV below the conduction band edge. Table 1.6.1 and Figure 1.6.1 were redrawn from H. Fritzsche[27] to show the electrical properties of Sb-doped Germanium in the high concentration region where metallic impurity conduction occurs.

For samples with $N_D > 10^{17}$ atom/cm^3, Figure 1.6.1 shows resistivity curves 25 to 29 to have a resistance which is independent of temperature below 10 K. Table 1.6.1 shows a dramatic lowering of the activation energy for samples 25 to 29. Wolf and Compton[35] have also reported that germanium doped with antimony in the range of 1 to 2 x 10^{17} atoms/cm^3 exhibits a temperature independent resistance for temperatures less than 10 K. The donor concentration N_D mentioned above agrees well with McIrvine's critical impurity concentration of $N_C = 1.3 \times 10^{17}$ atom/cm^3 in n-type Germanium. This can be seen in Table 1.6.2.[33]

Sample 29 [22] has a room temperature resistivity equal to the resistivity at 2.5 K. Despite the small rise in resistivity near 77 K, sample 29 shows a temperature independent resistivity up to room temperature. Papers by Hung and Gliessman have also reported this type of behavior.[1, 25]

Debye and Conwell[36] performed resistivity measurements from 11 to 300 K on a set of n-type germanium samples doped with arsenic covering the range from intrinsic to degenerate.

Table 1.6.1 Donor concentration and resistivity temperature parameters of n-type germanium samples

Sample number	N_D (cm^{-3})	ε (10^{-3} eV)	298 K ρ Ω-cm	77 K ρ Ω-cm	2.5K ρ Ω-cm
1	5.3×10^{14}		3.68	0.488	
2	9.3×10^{14}		2.10	0.302	7×10^{11}
5	1.6×10^{15}	0.99	1.22	0.200	5.8×10^{9}
7	2.3×10^{15}	1.1	0.882	0.160	3.2×10^{8}
8	3.0×10^{15}	1.2	0.668	0.130	5.0×10^{7}
10	5.2×10^{15}	1.5	0.400	0.0913	5.6×10^{6}
12	8.5×10^{15}	1.6	0.245	0.0660	1.6×10^{6}
15	1.3×10^{16}	1.5	0.162	0.0529	2.6×10^{5}
17	2.4×10^{16}	1.2	0.0980	0.0416	3.2×10^{4}
18	3.5×10^{16}	1.1	0.0723	0.0360	6.1×10^{3}
20	4.5×10^{16}	0.99	0.0614	0.0340	1.6×10^{3}
21	5.5×10^{16}	0.85	0.0508	0.0315	1.9×10^{2}
22	6.4×10^{16}	0.74	0.0450	0.0306	3.4×10
23	7.4×10^{16}	0.42	0.0410	0.0296	5.0
24	8.4×10^{16}	0.18	0.0367	0.0280	1.0
25	1.2×10^{17}	0.056	0.0284	0.0261	2.87×10^{-1}
26	1.3×10^{17}	0.031	0.0257	0.0243	1.59×10^{-1}
27	2.7×10^{17}	0	0.0153	0.0185	3.2×10^{-2}
29	9.5×10^{17}	-0.01	0.00637	0.00755	6.3×10^{-3}

Taken from H. Fritzsche reference 27

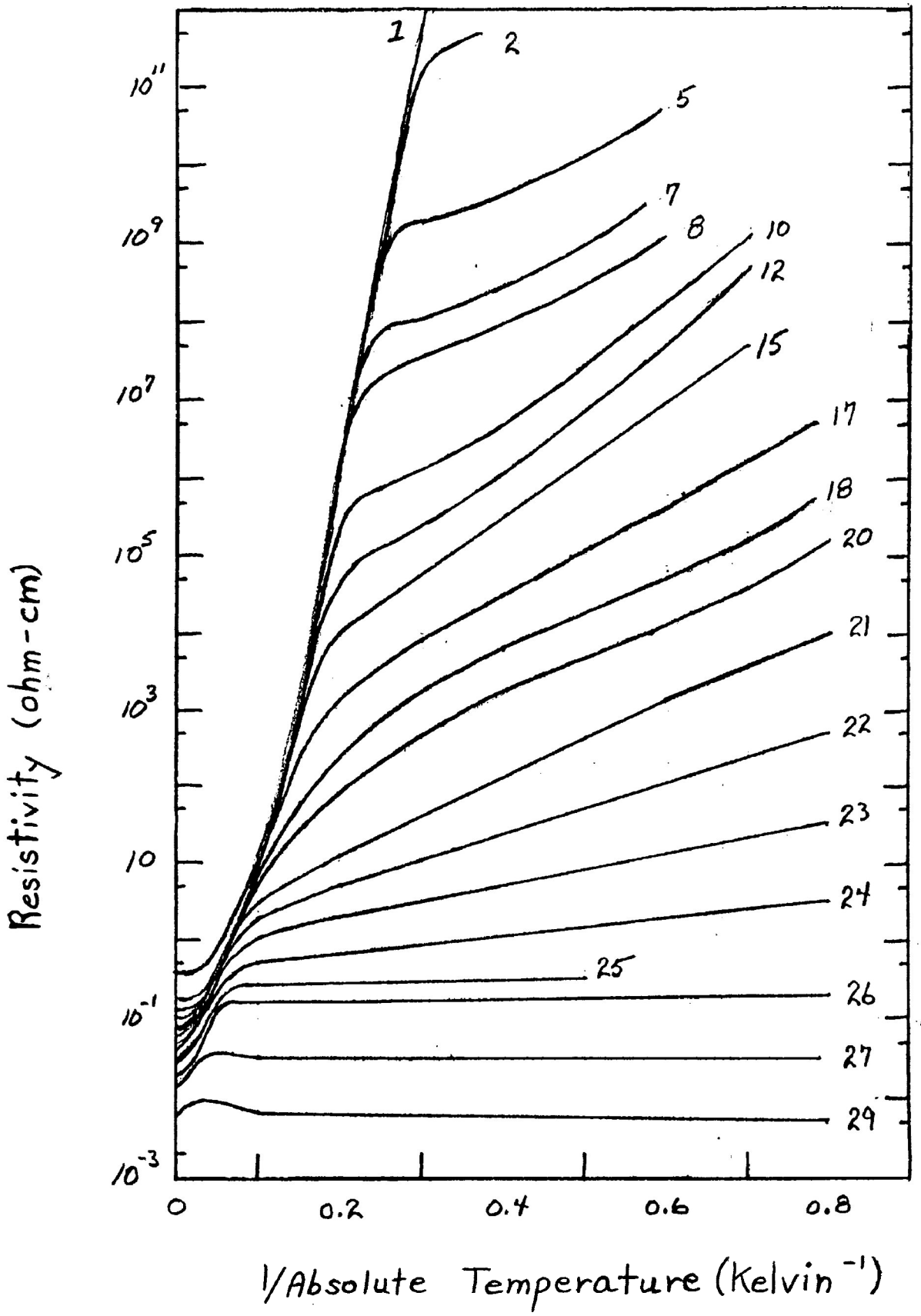

Figure 1.6.1 Resistivity of antimony-doped germanium (n-type) as a function of 1/T. Taken from H. Fritzsche reference 27

Table 1.6.2 Critical impurity concentration for a number of semiconductors

Material	$N_C(cm^{-3})$	ε
p-Mg_2Sn	$\sim 10^{16}$	19
p-InSb	1.3×10^{17}	16.0
n-Ge	1.3×10^{17}	15.8
p-Ge	1.4×10^{17}	15.8
n-Si	1.6×10^{19}	11.7
p-Si	6.5×10^{18}	11.7
n-CdS	$\sim 10^{18}$	11.6
n-SiC	$\sim 10^{20}$	10.0

Taken from E.C. McIrvine reference 33

Germanium doped with arsenic has a donor energy 0.013 eV below the conduction band edge. From 11 to 100 K there is almost no change in resistivity with temperature.

Silicon has an energy band gap of 1.12 eV at 300 K. Silicon doped with arsenic has a donor level equal to 0.049 eV below the conduction band edge.[34] Morin and Maita[37] measured the electrical properties of As-doped silicon in the high concentration region where metallic like impurity band conduction occurs. A temperature independent resistivity below 50 K was observed for an impurity concentration of 2.7×10^{19} atom/cm^3.

Pearson and Bardeen[38] have done electrical measurements on silicon doped with phosphorous over a temperature range of 87 to 900 K. At low concentration this produces a donor level 0.045 eV below the conduction band edge. Metallic like impurity conduction was observed to occur below 170 K for $N_D = 1.7 \times 10^{19}$ atoms/cm^3.

Cadmium Sulphide has an energy gap of 2.42 eV at 300 K.[39] Cadmium Sulfide crystals doped with chlorine has a donor ionization energy in the neighbourhood of 0.01 to 0.02 eV below the conduction band edge.[40] Toyotomi and Morigaki[41] show the electrical resistivity of Cl-doped Cadmium Sulphide in the high donor concentration region where a metallic like impurity conduction has been observed. At a donor concentration of $N_D = 2.1 \times 10^{18}$ atoms/cm^3, a temperature independent resistivity exists below 77 K.

J. Woods[42] reports on resistivity measurements for n-type ZnSe crystals ($E_g = 2.58$ eV) compensated with Indium (donor ionization energy = 0.2 eV)[43] in the temperature range of 70 to 300 K. Between 245 and 300 K the activation energy (about 33 meV) was found to decrease with indium compensation. Woods suggests that the conductivity is due to thermally assisted phonon tunneling between the localized donor states. The expression used is

$$\sigma = \sigma_0 \exp\left[-\left(E - E_F + \Delta W\right) / K_B T\right] \qquad \text{eq'n 1.6.1}$$

where $(E - E_F)$ is the activation energy required for raising electrons to an appropriate localized energy state E from the fermi level E_F. ΔW represents the hopping energy between two localized states.

Sebastian and Sivaramakrishnan[44] investigated electrical conduction in $CdSe_x\ Te_{1-x}$ (donor ionization energy between 0.3 and 0.5 eV)[45] in thin films between 125 and 300 K. Film compositions of $CdSe_{0.8}Te_{0.2}$ and $CdSe_{0.6}Te_{0.4}$ were found to be n-type. An activation energy of 0.02 eV was observed for both compositions below 290 K which is characteristic of phonon-assisted hopping conduction.

1.7 Background on Bismuth Iron Molybdate

Bismuth Iron Molybdate is used as a catalyst for the partial oxidation of olefins, for example the oxidation of propylene to form acrolein.[5] Selectivity and sensitivity[4, 5, 46] over a wide range of hydrocarbons makes $Bi_3FeMo_2O_{12}$ an exceptionally active catalyst by providing appropriate sites for adsorption. The catalyst acts as both a source and sink for oxygen and electrons.

The removal of lattice oxygen[47] from $Bi_3FeMo_2O_{12}$ is a redox reaction because the catalyst itself acts as an oxidizing agent. This redox concept is supported by showing the oxidation of propylene in the absence of gaseous oxygen. The oxygen appearing in the products comes from the participation of many sublayers of lattice oxygen in $Bi_3FeMo_2O_{12}$. A fast surface reduction leaves the boundary layers near the surface in a reduced state. This is followed by the diffusion of lattice oxygen to the surface. Lattice oxygen diffusion[48] and vacancy diffusion are identical except for sign. The diffusion gradient follows from the solution of Fick's Law

$$\partial C/\partial t = D\nabla^2 C \qquad \text{eq'n 1.7.1}$$

where C is the concentration of oxygen atoms or vacancies and D is the diffusion constant.

Pressed pellets of $Bi_3FeMo_2O_{12}$ powder show rapid and reproducible changes in electrical conductance at temperatures between 620 and 820 K on exposure to reducing vapour because oxygen vacancies act as donors. Air or gaseous oxygen serves to reoxidize the reduced catalyst causing the conductance to return to its original value.

Bismuth Iron Molybdate clumps together under pressure, for example when made into a pellet, but is still porous enough to allow air or a reducing vapour such as methanol to penetrate into the pellet interior. The three dimensional[49] network of grains consists of three distinguishable regions. The first is the surface gas interface where adsorption and desorption of physiadsorbed and chemiadsorbed vapours take place. Second is the near surface where the reduction of lattice oxygen produces oxygen vacancies within a hundred layers or so inside the solid particles or grains. Since the diffusion constant for oxygen vacancies is relatively fast (i.e., 7.7×10^{-14} cm^2 sec^{-1} at 687 K for the compound bismuth

molybdate)[48] one would expect a near surface reduction to some degree. The last region is the solid particle bulk which acts as a reservoir for lattice oxygen. These regions can be seen in Figure 1.7.1.

Bismuth Iron Molybdate powder is yellow in color and has an ordered scheelite superstructure related to the ideal scheelite structure formula AMO_4. The superstructure is due to the ordering of the Fe and Mo atoms on the M site of AMO_4. The ideal symmetry for a scheelite structure is a body centered tetragonal, but $Bi_3FeMo_2O_{12}$ shows a body-centered monoclinic cell with cell dimensions a = 16.155 Å, b = 5.254 Å, c = 11.652 Å and γ = 90.96 degrees. The standard C-centered cell is a = 16.904 Å, b = 11.652 Å, c = 5.254 Å, and β = 107.15° with space group C 2/C. The crystallographic density is 7.16 g/cm^3.[50,51]

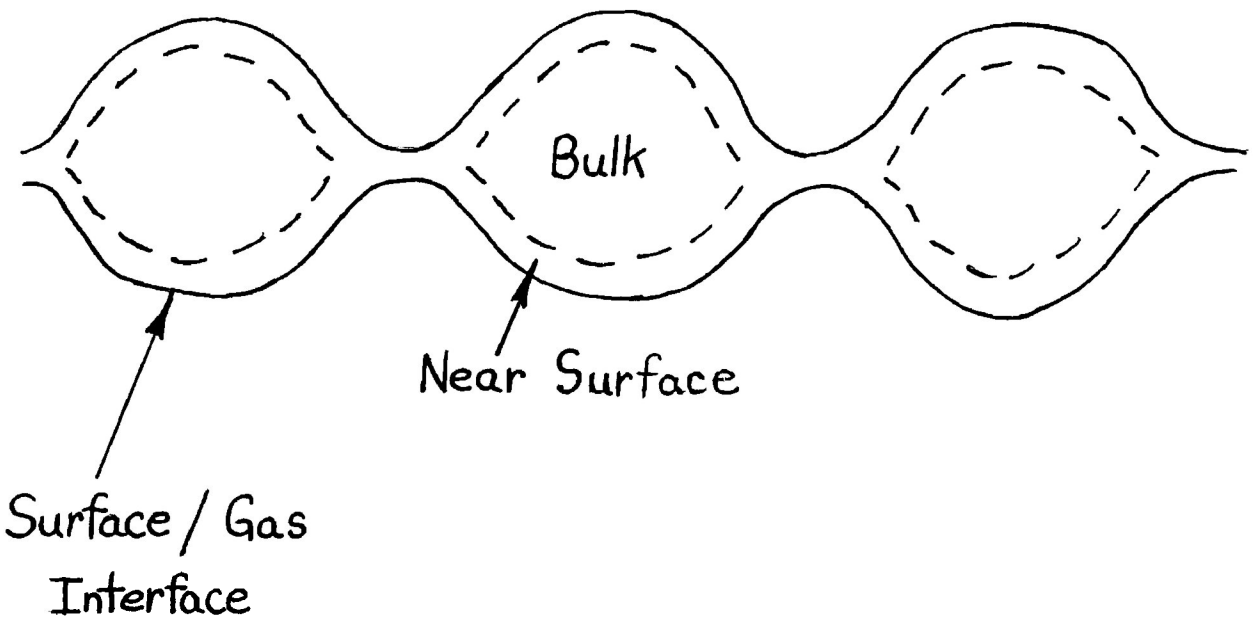

Figure 1.7.1 Bismuth Iron Molybate Network. Taken From Reference 40

CHAPTER 2
EXPERIMENTAL METHODS

2.1 Preparation and Chemical Reduction of $Bi_3FeMo_2O_{12}$ Pellets

Commercially obtained Bismuth Iron Molybdate ($Bi_3FeMo_2O_{12}$) powder was compressed with a pressure of 2.0×10^8 N/m^2 by a specially designed press to produce a 6 mm x 6 mm x 2 mm pellet weighing approximately 0.4 grams. This generates a sample density of 4.1 g/cm^3. The press allowed four evenly spaced 0.1 mm diameter gold wires to be embedded through the pellet center perpendicular to the vertical axes (refer to Figure 2.1.1).

The pellets were then heated in air at 670 K for ten hours inside a NEY 2-525 box furnace. After a two hour cooling period the samples were ready to be reduced in a methanol-nitrogen atmosphere.

The pellets were mounted in an enclosed stainless steel oven using silver dag to make electrical contact between the gold wires and insulated chromel wires which extended from the oven interior to external electronic equipment. A Keithley model 487 picoammeter/voltage source and a model 617 electrometer were used to monitor the conductance of the pellet during reduction by simultaneously measuring the voltage and current. The temperature of the oven was controlled by heating tape and a chromel-alumel thermocouple connected to an electronic controller. The oven was heated to 620 K for twelve hours to remove surface contaminants which accumulate on the pellet. This ensures immediate chemical reduction of the pellet when exposed to a reducing methanol/nitrogen atmosphere.

A regulated flow of nitrogen gas was bubbled through liquid methanol under atmospheric pressure. This introduces methanol vapour into the flow of nitrogen gas to yield a 13.2% methanol concentration. Methanol under 1 atmosphere at 300 K has a vapour pressure of 100 torr. Nitrogen at 300 K under one atmosphere is 760 torr. Thus (100/760) x 100% equals 13.2%. A flow of 100 ml/min of methanol/nitrogen gas entered the interior of the 100 ml oven through a 2.5 mm diameter tube. Switching this flow line

Figure 2.1.1

Schematic representation for measuring conductance or resistance inside the pellet

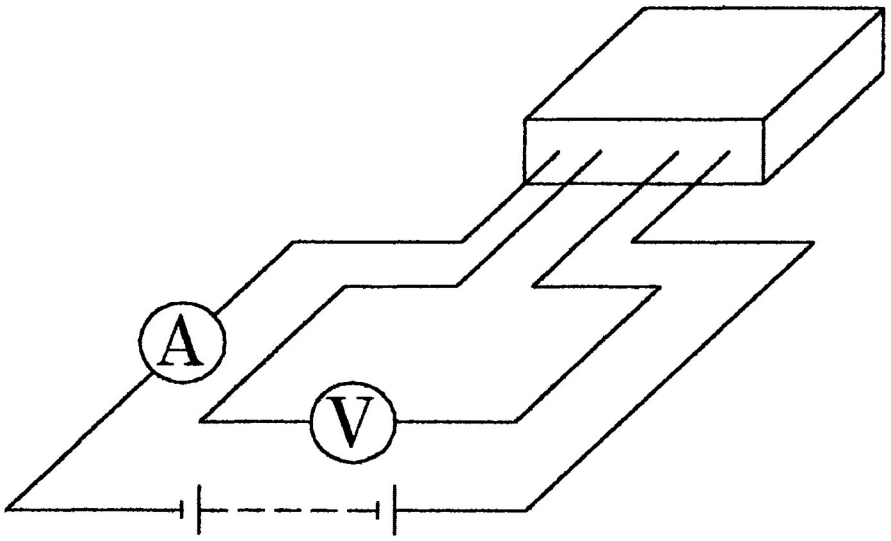

(pulsing) permitted 100 ml/min of oxygen free nitrogen carrier gas to enter the oven's interior instead. All samples were reduced by pulsing. Pulsing permits each pellet to achieve a desired conductance by first exposing it to the reducing atmosphere and then switching to pure nitrogen to allow the conductance to stabilize.

A real time computer data acquisition program displayed the logarithm of conductance versus time. Pulses varied from 30 seconds to 3 minutes for reduction and 30 seconds to an hour for stabilization. Total elapsed time ranged from 1.5 to 4.5 hours.

Figure 2.1.1 shows a schematic circuit for measuring conductance inside the pellet. The potential difference developed across the inner two probes is measured using a high input impedance voltmeter or electrometer. In this way the metal semiconductor contact resistance does not affect the results.

Once reduction and stabilization were completed satisfactorily the pellets were cooled in the oven from 620 K to room temperature in a nitrogen atmosphere. The resistance was measured as a function of temperature during this cooling.

The pellets were then mounted in a pour fill cryostat which was evacuated over a 16 hour period. The cryostat was rapidly cooled to liquid nitrogen temperature and then allowed to slowly warm up to room temperature. The resistance was measured as a function of temperature during this warming period. The basic layout of the cryostat is shown in Figure 2.1.2.

The 500 ml liquid nitrogen dewer, open to the atmosphere, is made of very thin stainless steel tubing. This permits the sample, mounted on a copper bar, to be cooled by conduction. The sample warms slowly after removal of the liquid nitrogen. The sample was held fast to the copper bar by a high vacuum silicon grease. Silver dag was used to electrically connect the four gold leads from the pellet to exterior electronics. A chromel-alumel thermocouple, stationed near the base of the copper bar was connected to an external monitor in order to record changes in the temperature of the pellet.

The cryostat exterior was constructed of a brass pipe, a circular brass plate and a set of six bolt brass flanges. The central brass flange housed a rubber o-ring for quick and

Figure 2.1.2 Cryostat Apparatus

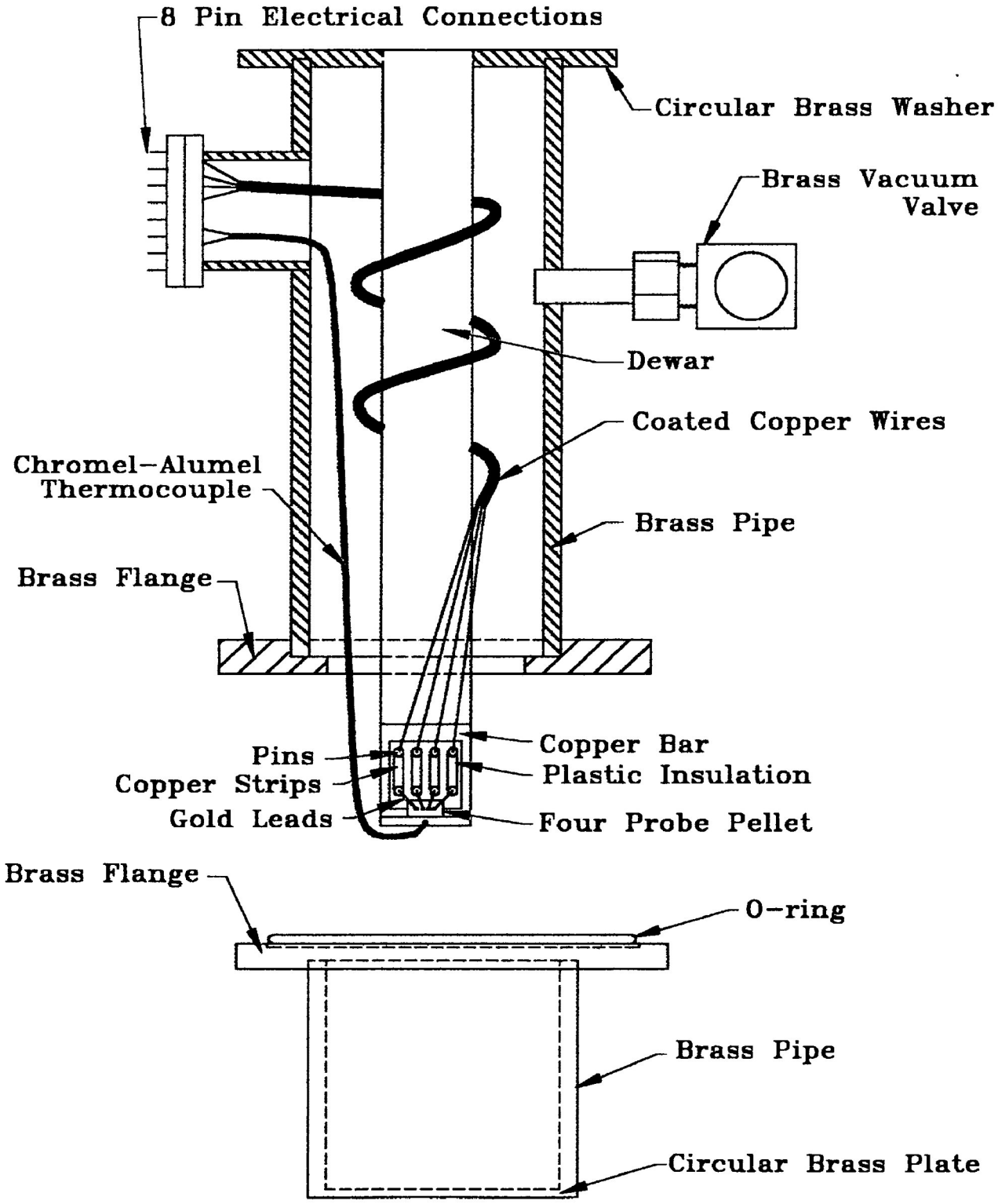

easy assembly and disassembly of apparatus. A vacuum valve permitted evacuation of the cryostat chamber once it was attached to the vacuum station.

2.2. Vacuum Station

Figure 2.2.1 shows the basic layout of the vacuum pumping station used in this project.[52] The vacuum vessel and various pumping lines are constructed of copper tubing. The brass flanges use embedded rubber o-rings to form air tight seals. Two thermocouple vacuum gages and an ionization gage are used for assessing vacuum conditions inside the vessel and roughing lines. The vapour diffusion pump connects to the high vacuum line directly below the cold trap and high vacuum valve. The diffusion pump uses an electric coil to heat and vapourize the oil. The cooling system allows water to flow through a metal coil soldered around the exterior wall of the pump casing. This causes the oil vapour to condense on the interior wall and flow back to the coil for reheating. The diffusion pump can sustain a pressure of 10^{-6} in the high vacuum line in approximately 30 minutes with continual back pumping.

The cold trap located above the diffusion pump and below the high vacuum valve should be filled with liquid nitrogen when the pressure in the high vacuum line has stabilized at approximately 10^{-6} torr. The liquid nitrogen cold trap acts as a catch basin to condense more water vapour within the high vacuum line. This type of cryogenic pumping lowers the pressure within the working chamber even further. As water vapour condenses, it forms a layer of ice on the cold surfaces of the cryogenic pump. This ice layer now acts as an insulator so the temperature on the outside of the ice layer is higher than the temperature of the refrigerant thus rendering the pump less efficient.

Pressures of 10^{-7} torr or better can be sustained for periods of ten to twelve hours without refilling. The roughing line valve is completely closed during full operation of the vacuum system. Access to the working chamber requires complete closure of the high vacuum valve and opening of the vessel's bleeder valve to permit removal of a circular steel cover. Once removed the port provides a direct means for evacuating the internal chamber within the cryostat through the high vacuum line.

Figure 2.2.1 Vacuum Station

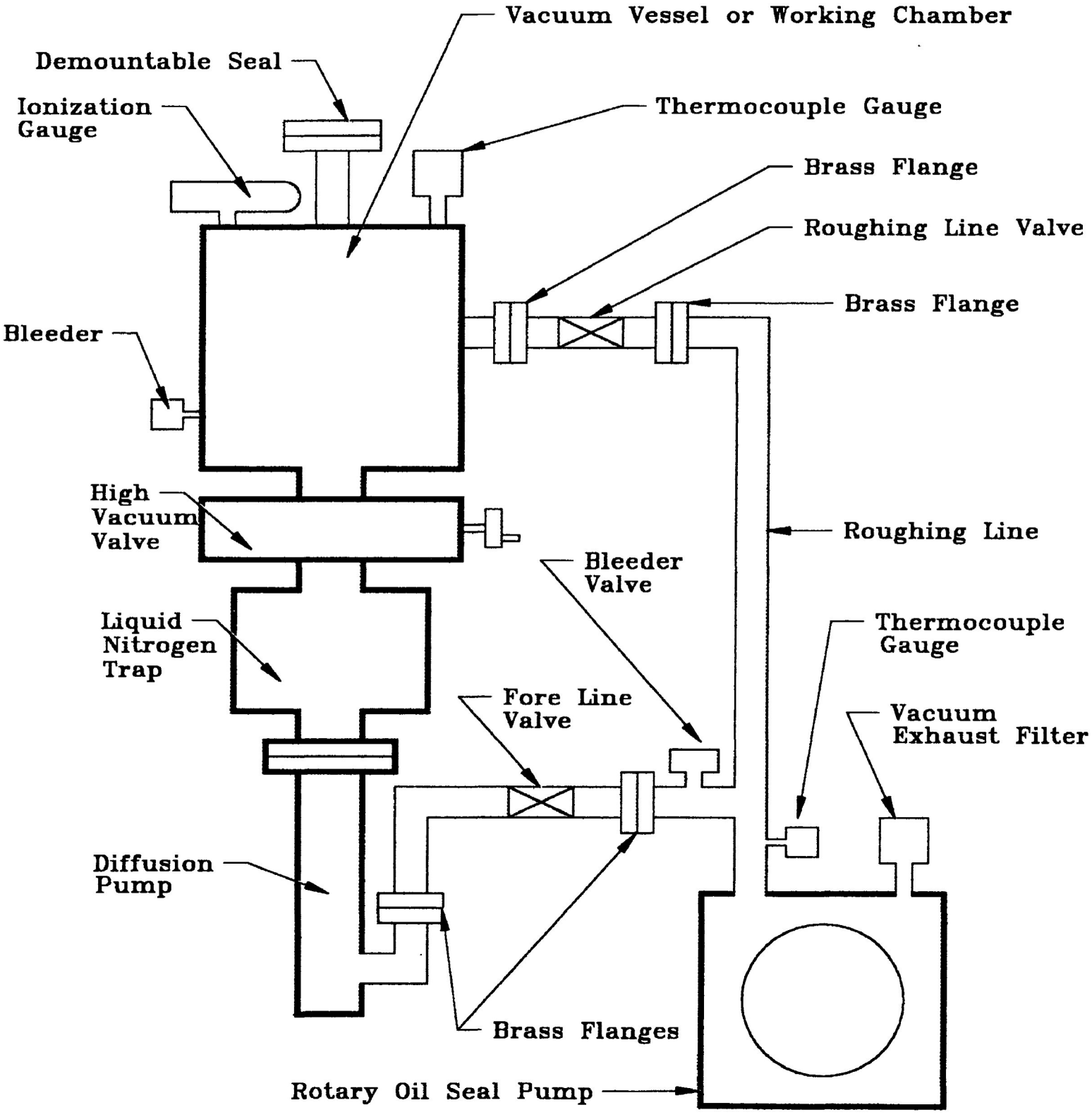

A bleeder valve soldered into the low vacuum line is used to relieve unwanted pressure on the oil seal of the mechanical pump during shutdown. This precautionary measure avoids the risk of damaging the seal and allowing oil from the pump to be drawn throughout the vacuum line to contaminate the entire system.

2.3 X-Ray Diffraction Measurements

X-Ray diffraction measurements performed on commercially obtained bismuth iron molybdate powder confirmed an ordered monoclinic superstructure cell.[50, 51]

X-Ray measurements done on reduced samples four through sixteen were prepared by grounding the samples with a mortar and pestel. A strip of double sided tape, covered uniformly with a powdered sample was held fast to a glass slide which was cut to fit inside the diffractometer. The powder diffractometer used was equipped with a copper target (CuKα radiation wavelength is 1.5418 Å) and was set to scan the angles 5 through 100 degrees at a resolution of 20 data points per degree.

CHAPTER 3

RESULTS AND DISCUSSION

3.1 Reduction in Methanol/Nitrogen Atmosphere

Figure 3.1.1, 3.1.2 and 3.1.3 shows the variation in conductance versus time for pellets of bismuth iron molybdate exposed to various pulses of 13.2% methanol in nitrogen at 620 K. Table 3.1.1 gives the conductance for each pellet thus reduced.

Sample 16 in Figure 3.1.3 shows the conductance approaching an equilibrium value near 10^{-6} seimens. Since this pellet was reduced in a pure nitrogen atmosphere (i.e., no methanol) only surface oxygen was removed.

The initial sharp rise in conductance for sample 15 to 3.2×10^{-4} seimens is due to chemical reduction in methanol vapour. This is followed by a pulse of nitrogen gas which allowed the conductance to stabilize. Air was subsequently introduced to suppress the pellet conductance.

Samples 4 to 14 were all chemically reduced with pulses of methanol vapour, intermittently switching to pure nitrogen to stabilize the pellet conductance. Samples 4 to 14 were not exposed to air during the reduction process. These samples were all attempts to produce a final conductance between 10^{-4} and 10^{-1} seimens.

Figure 3.1.1
Chemical reduction of pellets 4 to 8

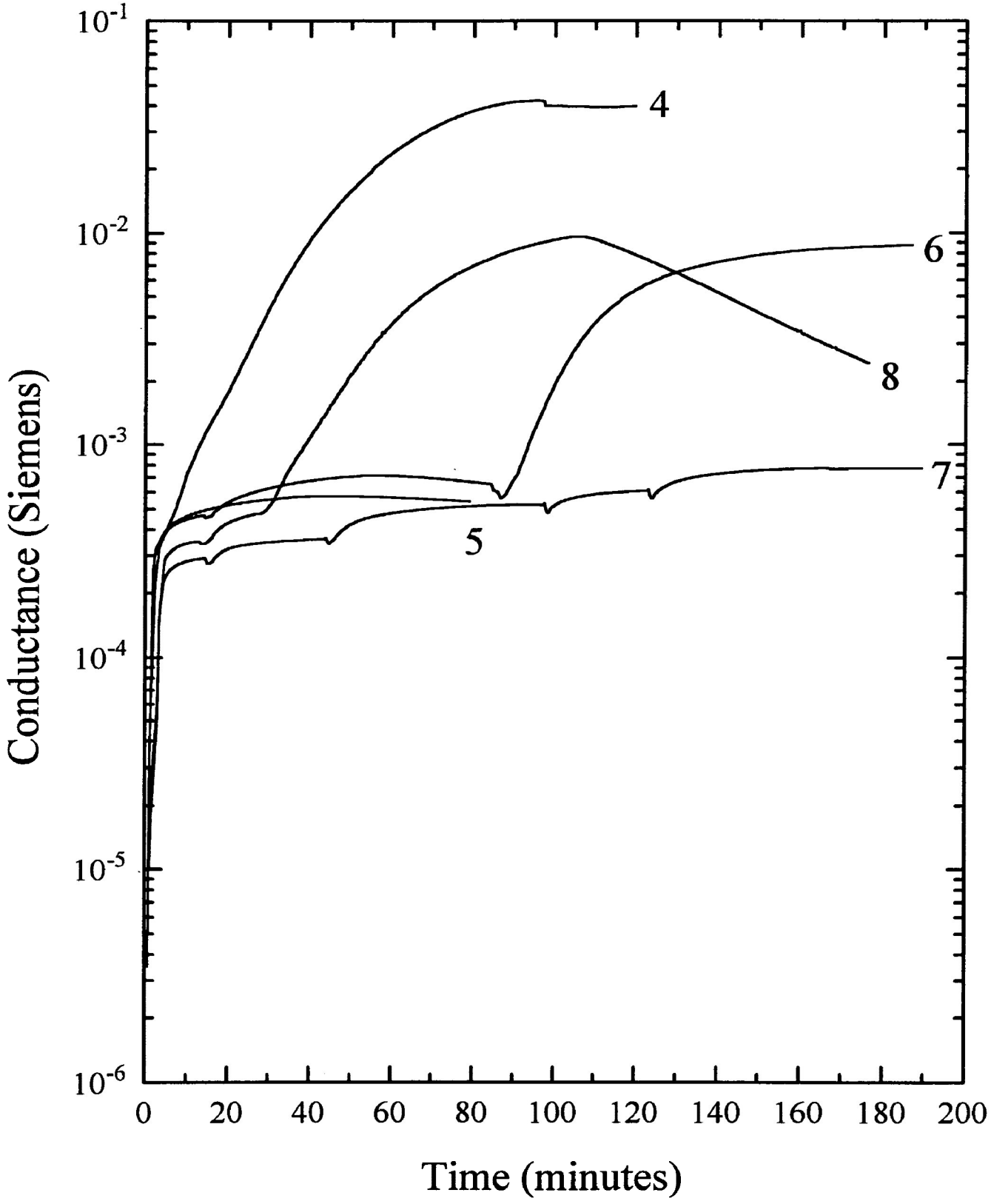

Figure 3.1.2
Chemical reduction of pellets 9 to 13

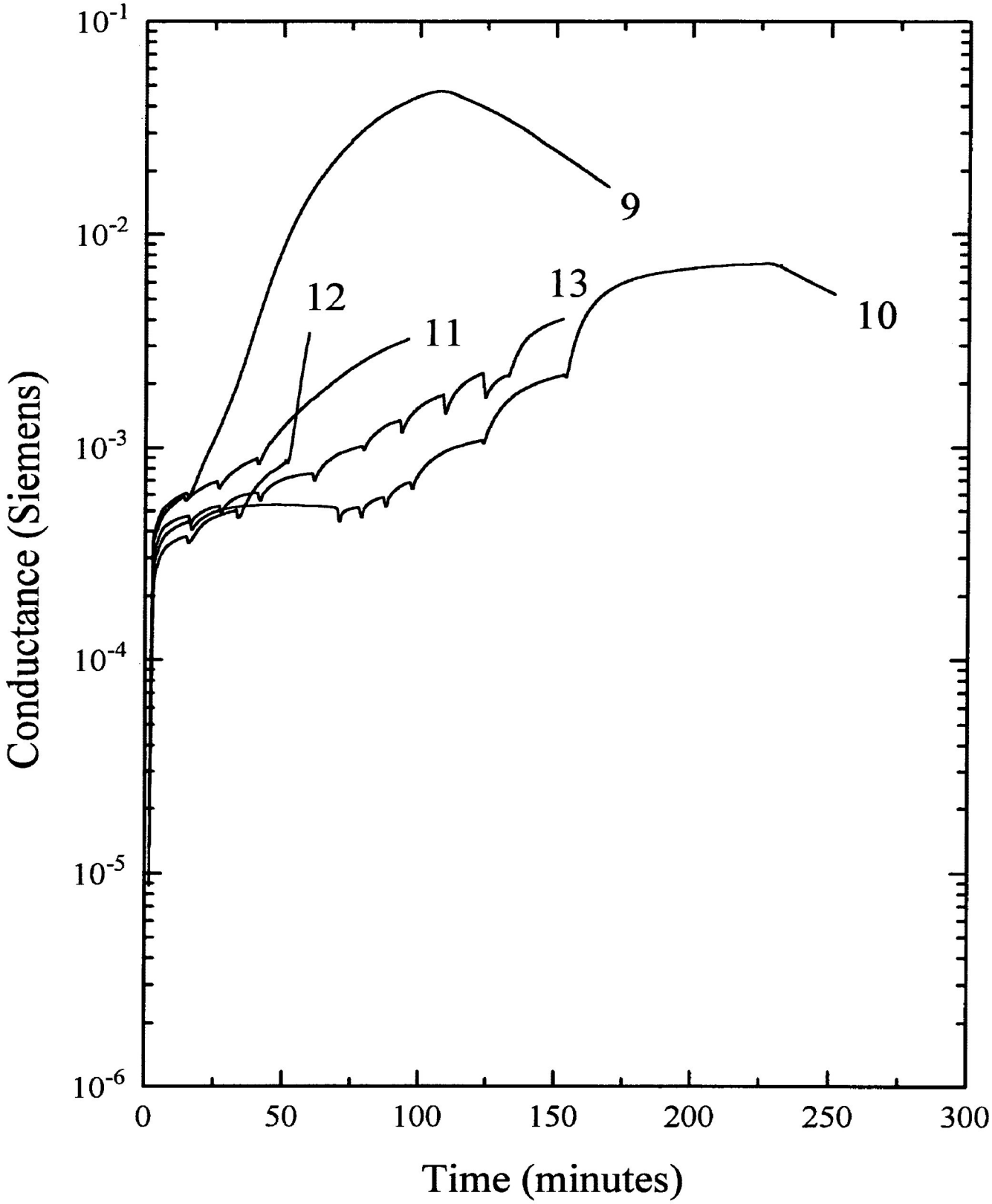

Figure 3.1.3
Chemical reduction of pellets 14 to 16

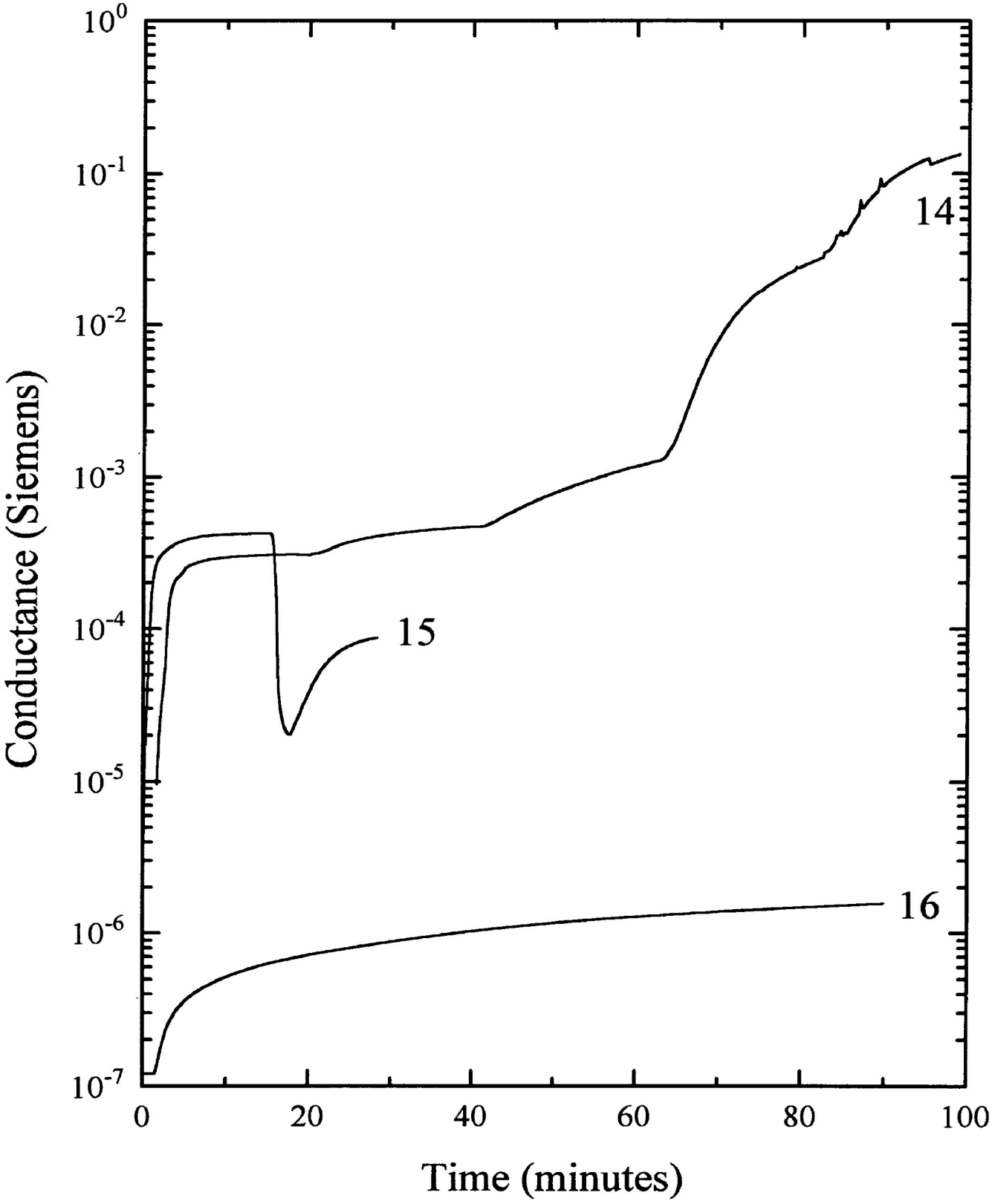

Table 3.1.1 Conductance of $Bi_2FeMo_2O_{12}$ pellets at 620 K after chemical reduction

Sample Number	Final Conductance (Siemens)	Final Resistance (ohms)
16	1.6×10^{-6}	641,000
15	8.7×10^{-5}	11,500
5	5.4×10^{-4}	1840
7	7.7×10^{-4}	1300
8	2.4×10^{-3}	412
11	3.2×10^{-3}	310
12	3.4×10^{-3}	290
13	4.0×10^{-3}	249
10	5.2×10^{-3}	190
6	8.7×10^{-3}	114
9	1.7×10^{-2}	60
4	4.0×10^{-2}	25
14	1.3×10^{-1}	7.5

3.2 Cooling and Low Temperature Analysis

Figure 3.2.1 shows the temperature dependence of the open circuit resistance in the evacuated cryostat with no sample present. This resistance is due to the conductance through the plastic insulation holding the contact pins. As a result the resistance measurements of samples 16, 15, 7 and 5 were discontinued before the level shown in Figure 3.2.1 was reached.

Figures 3.2.2, 3.2.3 and 3.2.4 show the temperature dependence of pellet resistance measured after switching off the oven and allowing the pellet to cool to room temperature in a nitrogen atmosphere followed by the temperature dependence of the pellet resistance as it warmed from 90 K to room temperature in a vacuum cryostat.

Figure 3.2.3 shows discontinuities in the conductance of samples 4, 6, 10 and 14 near room temperature. This could be due to chemisorbed vapour on the granular surafaces that could not be removed during the evacuation period.

Figure 3.2.1

Open circuit resistance of the cryostat

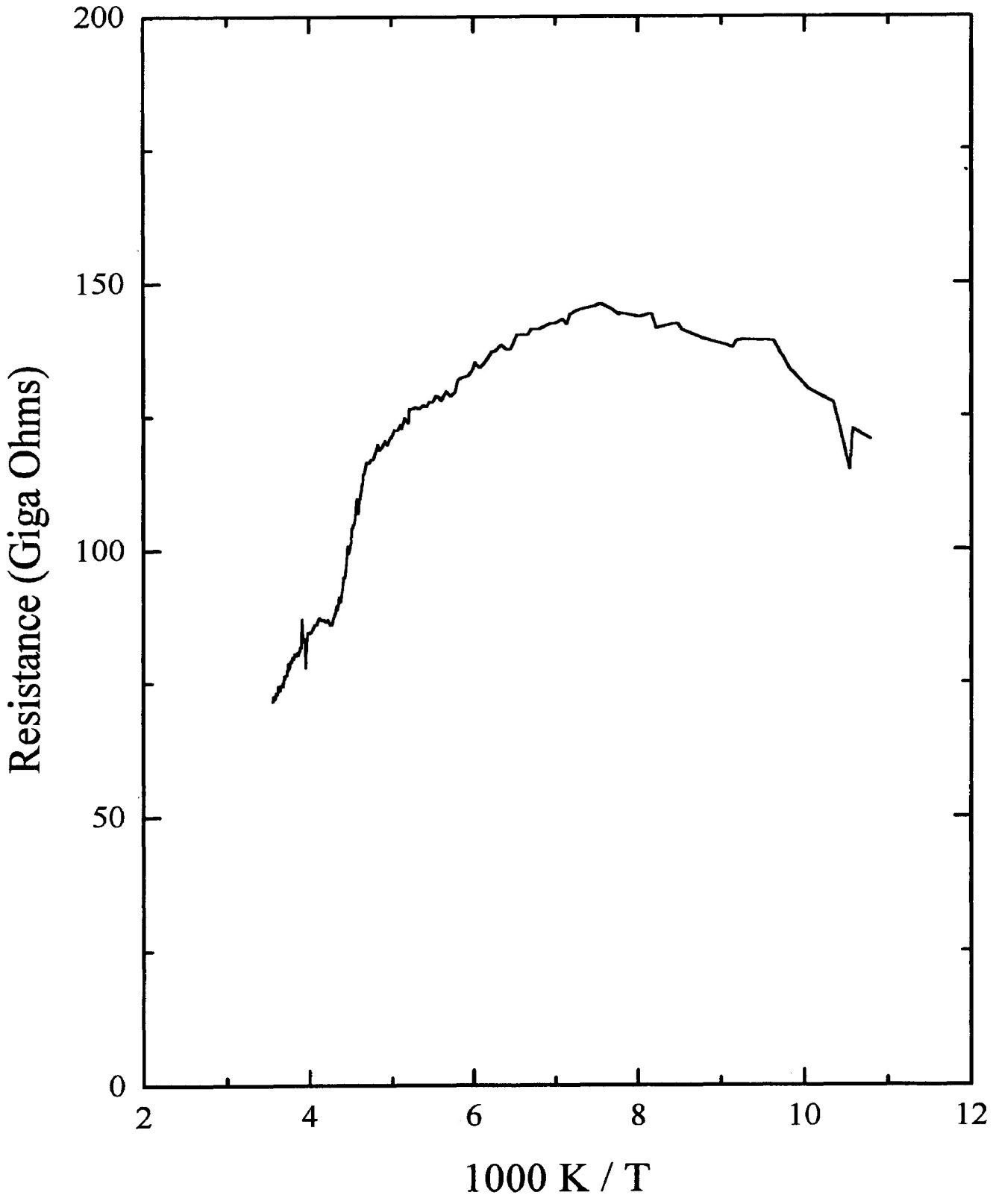

Figure 3.2.2

Temperature dependence of resistance for pellets 4 to 16

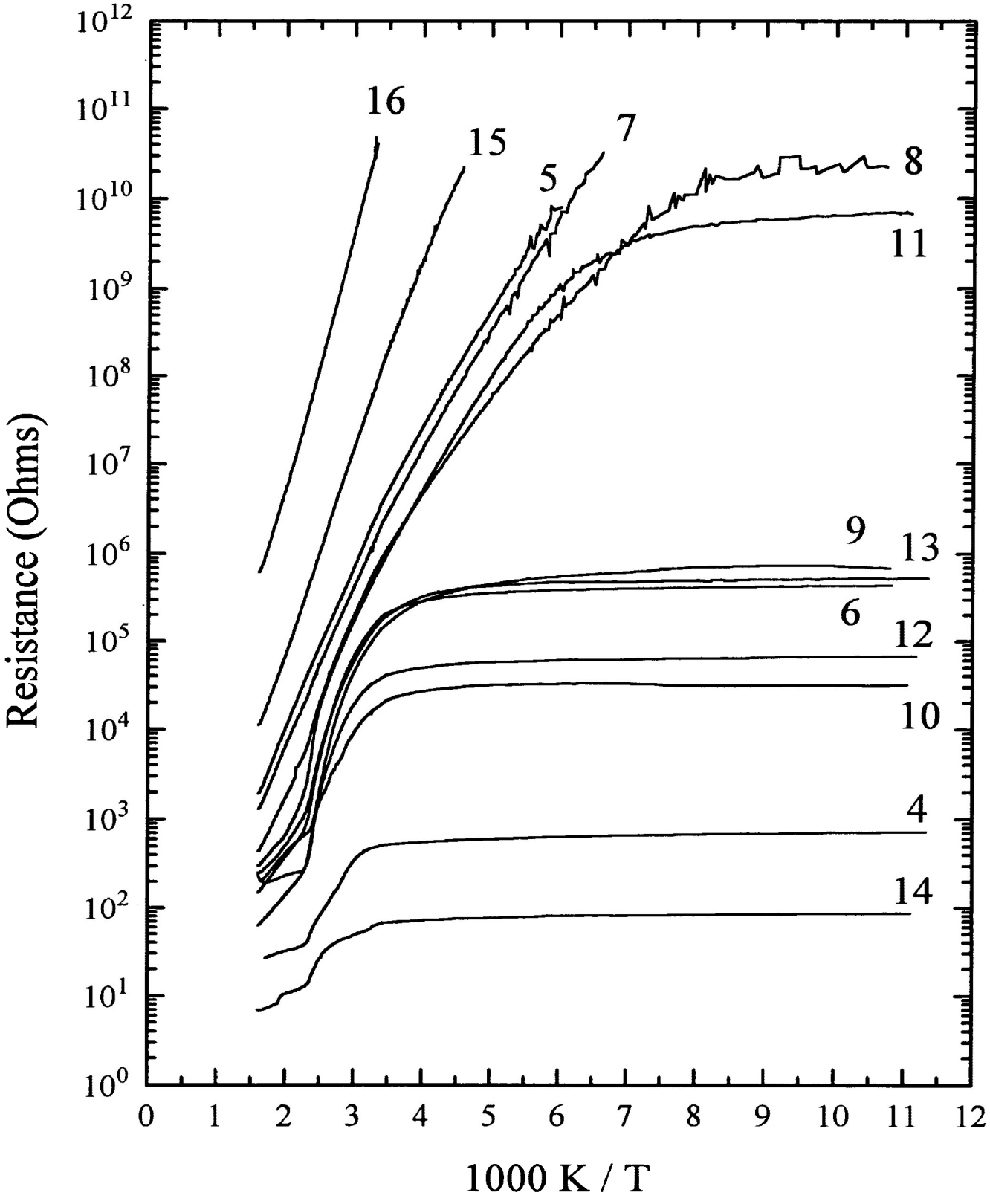

Figure 3.2.3

Temperature dependence of resistance for pellets indicated

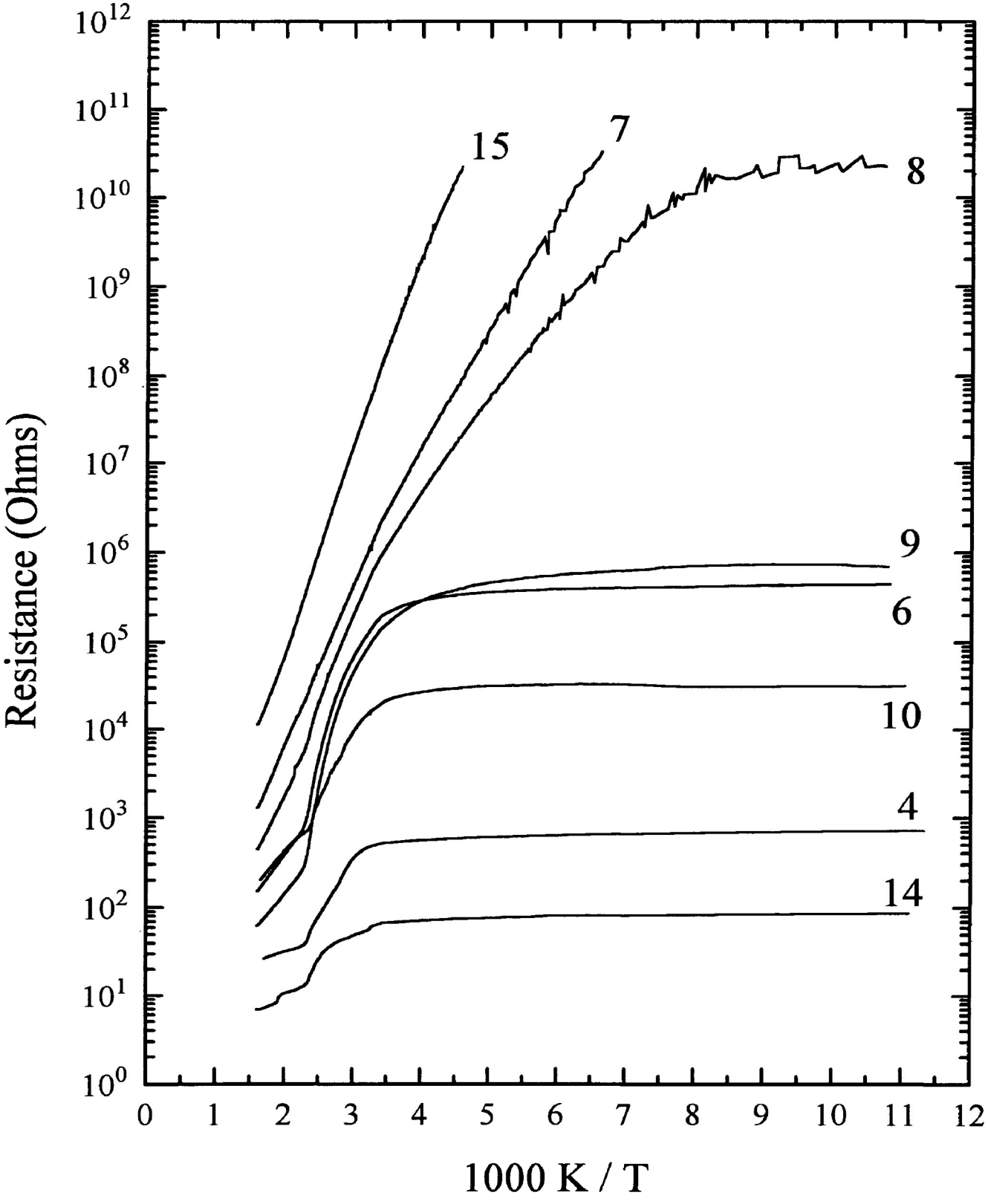

Figure 3.2.4

Temperature dependence of resistance for pellets indicated

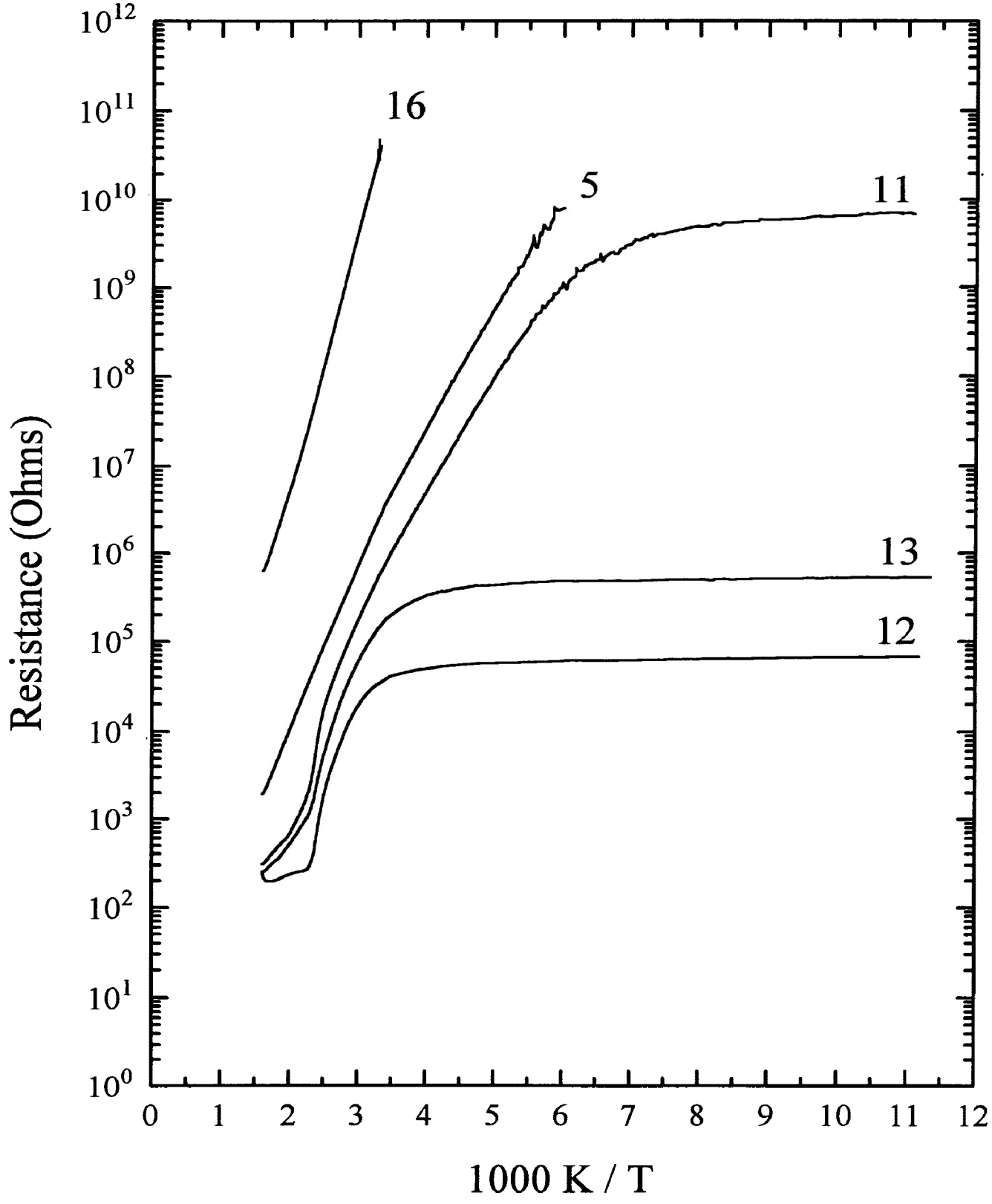

Equation 1.3.4 gives the conductivity for electrons in the conduction band in the temperature range of 90 to 300 K and is restated below.

$$\sigma_L = 2eB_1\left(\frac{2\pi m_e K_B}{h^2}\right)^{3/2} \exp\left(\frac{E_D - E_C}{K_B T}\right) = \sigma_1 \exp^{-\varepsilon_1/K_B T} \qquad \text{eq'n 3.2.1}$$

When comparing this equation to equation 1.4.1 for hopping conduction in the impurity band we see an exponential similarity as restated below.

$$\sigma_{IBC} = \sigma_2 \exp^{-\varepsilon_2/K_B T} \qquad \text{eq.n 3.2.2}$$

Thus at high temperature σ_L will dominate and at low temperature σ_{IBC} will dominate as $\varepsilon_1 >> \varepsilon_2$ and $\sigma_1 >> \sigma_2$. In either case

$$\rho = \frac{1}{\sigma} = \rho_o \exp(\Delta E / K_B T) \qquad \text{eq'n 3.2.3}$$

The equation used to fit the linear portions or the straight line segments of the resistance curve in the temperature ranges where a single exponential term dominates is,

$$\log_{10} R = a + b\left(\frac{1000K}{T}\right) \qquad \text{eq'n 3.2.4}$$

where a will involve ρ_o as well as the geometric dependence of the resistance and b will be directly related to the activation energy ΔE. That is

$$\Delta E = \frac{bK_B\, 1000K}{e\ \log_{10} e} = (0.1987)b \qquad \text{eq'n 3.2.5}$$

where ΔE is expressed in electron volts. Equation 3.2.5 was used to calculate all the activation energies listed in this thesis.

Table 3.2.1 lists samples with low impurity concentrations. The activation energy for sample 16 represents the energy level at which physisorbed and chemisorbed oxygen reside relative to the conduction band edge.

The most probable energy level for oxygen donor impurities at low concentrations appears to be centered about 0.36 eV below the conduction band edge.[27]

Table 3.2.1 Activation energies for low impurity donor concentrations in the high temperature range.

Sample Number	Temperature Range (K)	Activation Energy (meV)
16	300 - 620	580
15	300 - 620	490
5	300 - 620	360
7	300 - 620	360
8	300 - 380	360
11	300 - 380	340

The samples of Table 3.2.1 are also shown in Table 3.2.2 but with activation energies measured over a lower temperature range. The change in activation energies is probably due to chemisorbed oxygen on the granular surfaces produced when the pellet was removed from the oven and transferred to the cryostat. Chemisorbed oxygen acts as a surface trap for electrons[46, 53] and thus lowers the activation energy. The vacuum station should remove phyisorbed oxygen but may not remove chemisorbed oxygen.

Table 3.2.2 Activation energies for low donor concentrations in the medium temperature range.

Sample Number	Temperature Range (K)	Activation Energy (meV)
15	220 - 290	390
5	160 - 290	260
7	150 - 290	260
8	140 - 290	210
11	170 - 290	250

Table 3.2.3 and 3.2.4 show the properties of samples which are believed to exhibit conduction through an impurity band. Here we see a few characteristic features which are common to all semiconductors that are highly doped with impurities.

Samples 8 to 14 in Table 3.2.3 are arranged according to increasing conductance as a result of chemical reduction. It is apparent that as a result of the reduction process,

the concentration of oxygen vacancy donors must also increase. All samples show very little change in resistance over the temperature region specified. This region also extends to higher temperature with increasing chemical reduction.

Table 3.2.4 shows a lowering of the activation energy with increasing chemical reduction.

Table 3.2.3 Near temperature independent resistance over the given temperature range

Sample Number	Temperature Range (K)	Resistance Range (ohms)
8	90 - 110	14 - 20 GΩ
11	90 - 120	5.3 - 6.0 GΩ
9	90 - 130	0.9 - 0.96 M Ω
13	90 - 190	0.45 - 0.52 M Ω
6	90 - 190	0.36 - 0.44 M Ω
12	90 - 220	57 - 69 kΩ
10	90 - 220	59 - 61 kΩ
4	90 - 290	0.7 - 0.91 kΩ
14	90 - 290	44 - 56Ω

Table 3.2.4 Activation energies for high donor concentrations in the low temperature range 100 to 120 K.

Sample Number	Activation Energy (meV)
8	15.9
11	9.2
9	1.3
13	1.6
6	1.9
12	2.0
10	1.2
4	1.8
14	1.0

3.3 X-Ray Powder Diffraction Measurements

Figure 3.3.1 is the x-ray powder diffraction spectra for bismuth iron molybdate powder. Table 3.3.1 lists the locations and normalized intensities of these peaks. The miller indices, hkl, are derived from the structure reported in the literature.[50, 51] This structure is given in section 1.7.

X-ray powder diffraction spectra were obtained for all samples but it is only necessary to show the section of intermediate interest of a few spectra. These sections are displayed as intensity versus diffraction angle in Figures 3.3.2, 3.3.3 and 3.3.4. Table 3.3.2 lists the d-spacings and normalized intensities for non $Bi_3FeMo_2O_{12}$ peaks. These peaks were normalized by the most intense peak at 3.180 Å, of $Bi_3FeMo_2O_{12}$.

Table 3.3.3 lists possible identifications for these new peaks. Appendix A tabulates the x-ray powder diffraction standards of the International Center of Diffraction Data (I.C.D.D.).

It is clear from Table 3.3.2 that only two new peaks are observed, one near 3.41 Å and one near 3.26Å. Table 3.3.3 indicates that bismuth, dibismuth trioxide (Bi_2O_3) and molybdenum trioxide (MoO_3) are in the vicinity of the newly formed peak centered about 3.26 Å. It is not clear which compound corresponds to the individual peak in each sample shown in Table 3.3.2. One would think that it must be one or another or perhaps portions of all three. The peak near 3.41 Å is most likely Molybdenum dioxide.

Figure 3.3.1

X-ray diffraction of bismuth iron molybdate

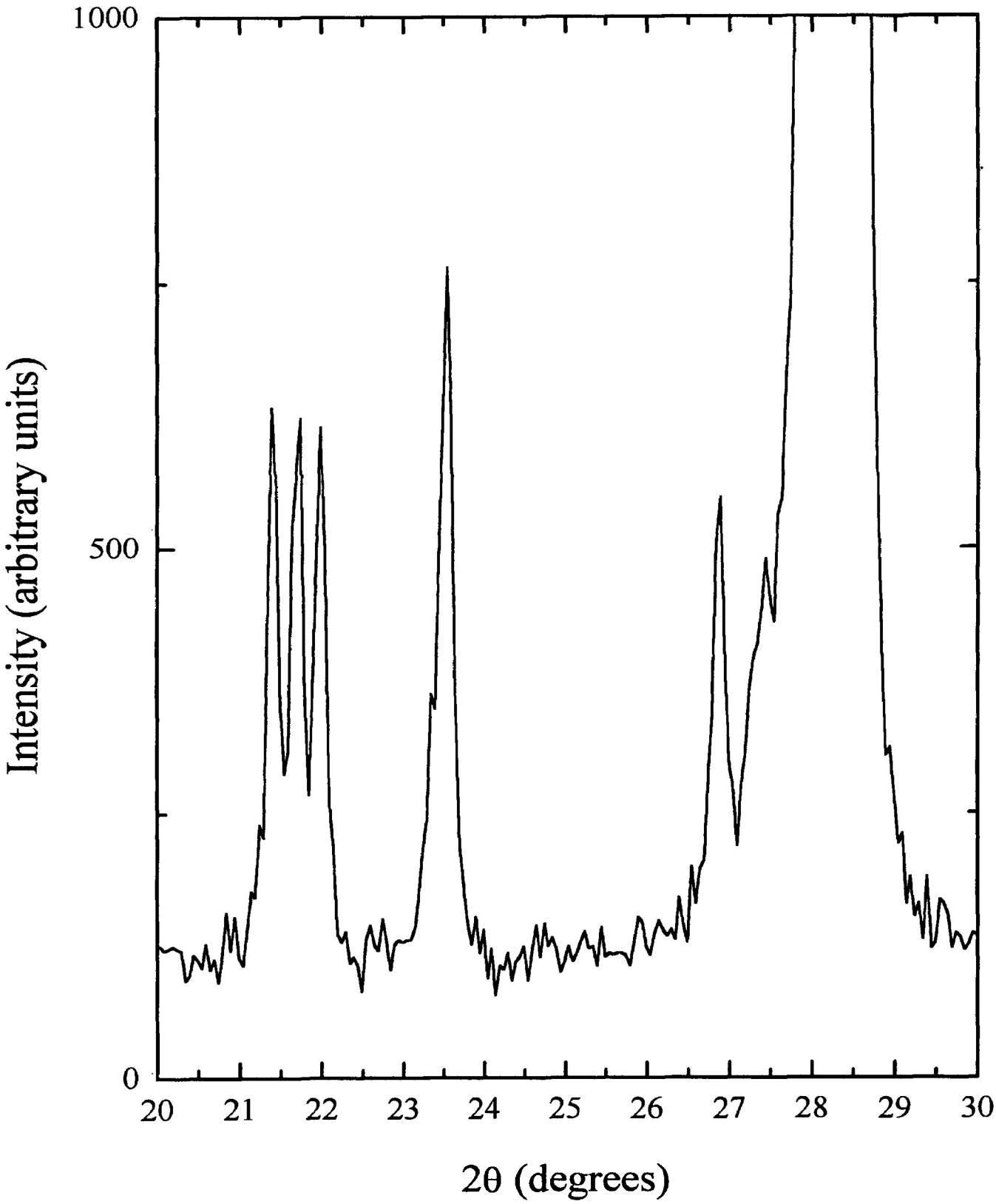

Table 3.3.1 X-Ray Powder Diffraction Pattern for $Bi_3FeMo_2O_{12}$

Peak	2 θ (degrees)	d-spacing (Å)	Normalized Intensities	*hkl
1	9.35	9.458	1	101
2	11.00	8.043	0.2	200
3	18.15	4.888	16	301
4	18.50	4.796	17	011
5	18.74	4.735	1	202
6	21.41	4.150	3	-211
7	21.76	4.084	3	211
8	22.00	4.040	3	400
9	23.35	3.810	0.1	-112
10	23.56	3.776	6	103
11	26.84	3.322	2	402
12	28.08	3.178	100	-312
13	28.43	3.139	99	312
14	30.70	2.912	30	004
15	33.26	2.694	32	600
16	34.11	2.628	17	020
17	35.71	2.514	7	114
18	36.17	2.483	8	-413
19	36.54	2.459	2	413
20	38.09	2.362	3	404
21	38.65	2.330	11	611
22	39.07	2.305	8	105
23	39.82	2.264	1	701
24	42.26	2.139	0.5	305
25	42.44	2.130	4	015
26	43.89	2.063	0.4	-215
27	44.01	2.057	0.2	215
28	44.20	2.049	6	-613
29	44.70	2.027	0.6	-323
30	44.83	2.022	1	800

*The hkl column was taken from reference 50

Figure 3.3.2
X-ray diffraction of pellet 11

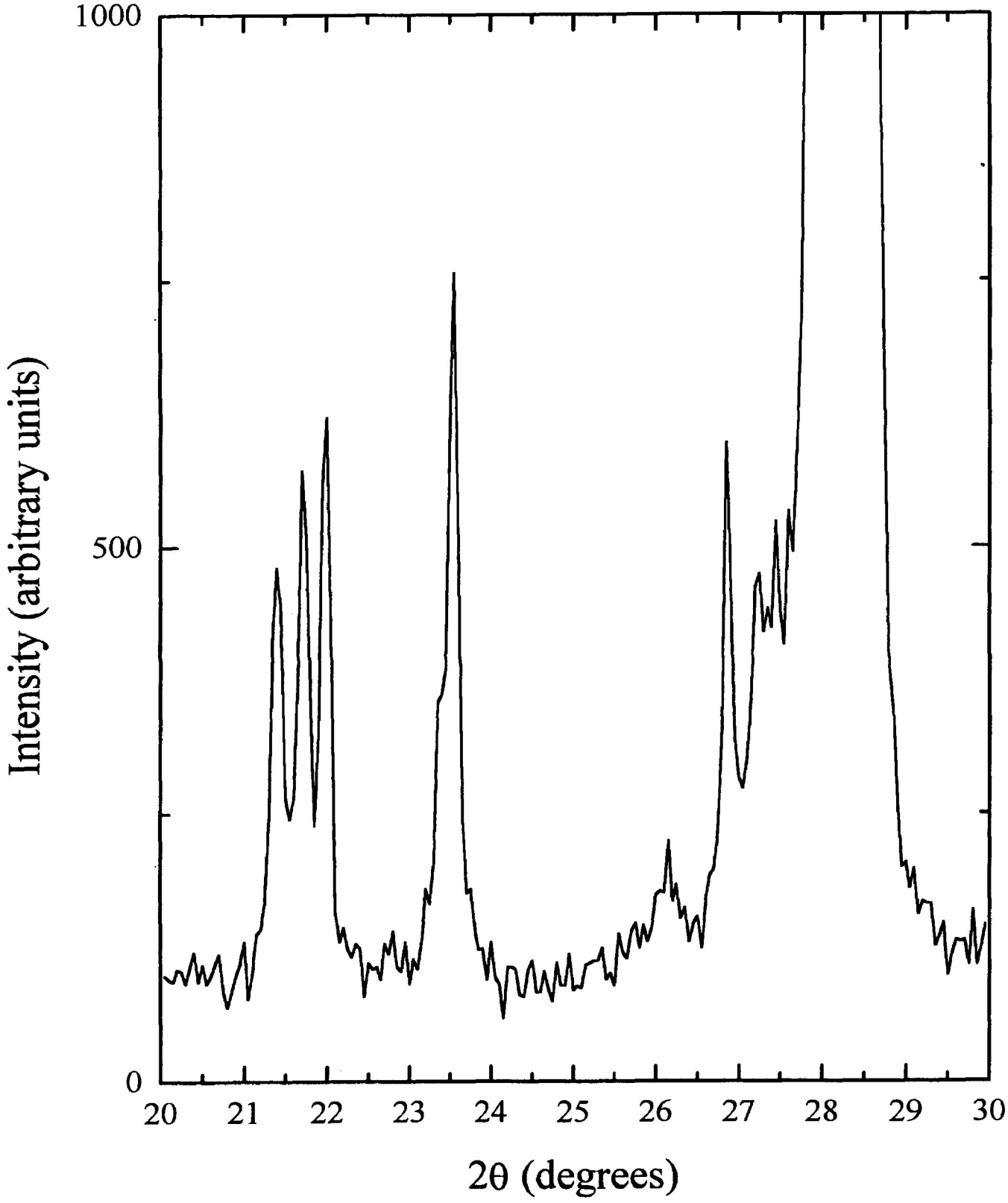

Figure 3.3.3
X-ray diffraction of pellet 6

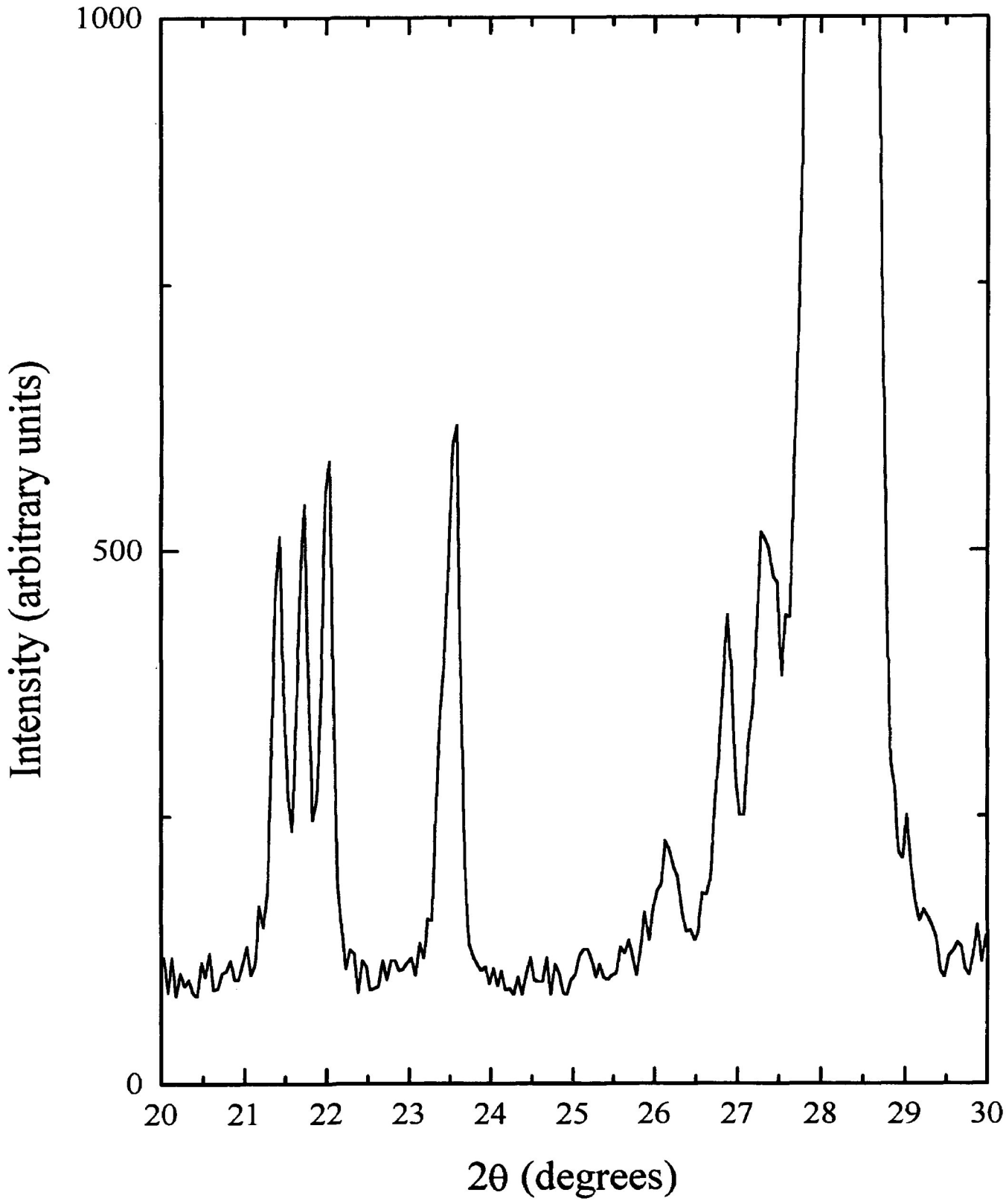

Figure 3.3.4
X-ray diffraction of pellet 14

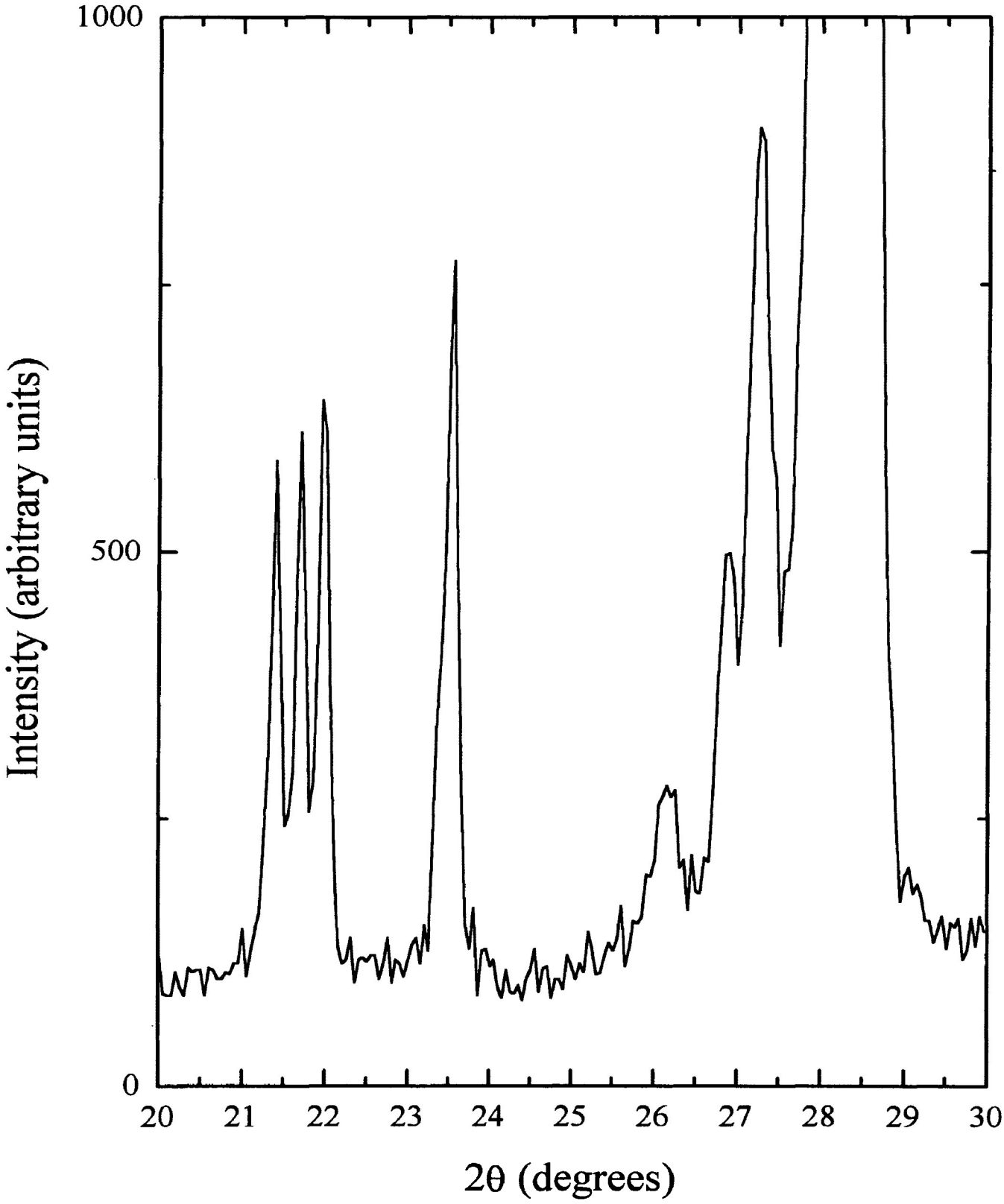

Table 3.3.2 New peaks observed in $Bi_3FeMo_2O_{12}$ as a result of chemical reduction.

Sample Number	2 θ (degrees)	d-spacing (Å)	Normalized Intensity
16	27.22	3.276	0.6
15	27.44	3.250	0.1
5	27.33	3.263	2
7	27.36	3.260	2
8	26.14	3.409	1
	27.31	3.265	1
11	27.28	3.269	1
9	26.18	3.404	1
	27.32	3.264	1
13	26.19	3.403	0.6
	27.32	3.264	1
6	26.18	3.404	1
	27.33	3.263	2
12	27.33	3.263	2
10	27.33	3.263	1
4	27.36	3.260	0.5
14	26.16	3.406	2
	27.28	3.269	8

Table 3.3.3 Possible compounds observed in $Bi_3FeMo_2O_{12}$ as a result of new peak formation.

d-spacings (Å)	Compound	*hkl
3.259	MoO_3	021
3.270	Bi_2O_3	111
3.280	Bi	012
3.420	MoO_2	-111

*The hkl column was taken from appendix A

CHAPTER 4

CONCLUSION

For lightly reduced pellets of bismuth iron molybdate (i.e., for low concentrations of oxygen vacancies) an activation energy of 0.360 eV was obtained over a temperature range of 300 - 620 K. We believe this represents the energy level of oxygen vacancy donors with respect to the conduction band edge. This is observed in Table 3.2.1 for samples 5, 7, 8 and 11.

The shift in activation energy given in Table 3.2.2 for the temperature range of 150 - 300 K is probably due to adsorbed water vapour or oxygen on the surface of the pellet when it was removed from the oven and transferred to the cryostat. These vapours have the ability to trap electrons at the surface and change the activation energy.[46, 53, 54]

Our resistance versus temperature curves suggest a metallic like conduction process at the low temperature region of the more heavily reduced pellets. Supporting evidence for this claim can be seen in the near temperature independent resistances shown in Table 3.2.3 and the low activation energies shown in Table 3.2.4.

As the oxygen vacancy donor concentration increases the temperature region dominated by the impurity band extends to higher temperature. Increased donor concentration suggests strong overlap of the electron wave functions about the impurity centers. The localization of the wave function is removed and electronic conduction occurs through a band of energy levels. At some concentration a transition from hopping to metallic like conduction takes place in the impurity band. With the impurity band located near 0.360 eV the contribution of extrinsic electrons in the conduction band would be $9.1 \times 10^{-5}\%$ of the donor electrons at 300 K. At 90 K it would be $7.4 \times 10^{-19}\%$. It is therefore likely that conduction through the impurity band will dominate due to the absence of electrons in the conduction band.

X-ray powder diffraction measurements indicate that bismuth, dibismuth trioxide and molybdenum trioxide are centered near the newly formed peak at 3.26 Å. This can be observed in Tables 3.3.2 and Table 3.3.3. Although pure bismuth exhibits metallic

conduction it is highly unlikely that the metallic like conduction observed in n-type $Bi_3FeMo_2O_{12}$ is due to the small amounts of pure bismuth formed, consistent with the magnitude of the X-ray peaks seen. Only for very heavily reduced samples is pure bismuth seen to sweat out of the pellet.[6,46,55] Sample 14 (i.e., the most heavily reduced sample) did not show this. It is therefore possible that the resistance result seen, at least in sample 14, could be due to a parallel network of a metallic layer on the semiconductor bulk. Dibismuth trioxide and molybdenum trioxide would not produce a metallic like conduction since these two compounds have an energy gap of approximately 1.0 eV.[56]

Molybdenum dioxide exhibits metallic conduction[57] at room temperature and has been identified as the peak centered at 3.41 Å in Figure 3.3.4 for sample 14. However all the other samples do not show this peak and therefore the low activation energies listed in Table 3.2.4 should be due to a hopping or metallic conduction through the impurity band and not to the existance of molybdenum dioxide.

Since 33 meV[42] and 20 meV[44] have been quoted as characteristic features of phonon assisted hopping conduction in the scientific literature for the compounds ZnSe doped with indium and $CdSe_xTe_{1-x}$ respectively the two activation energies listed in Table 3.2.4 for samples 8 (16 meV) and 11 (9 meV) could very well be of a hopping conduction process through the impurity band. The remainder of the samples in Table 3.2.4 have activation energies between 1 and 2 meV and should therefore indicate metallic like conduction in the impurity band.[25, 27] The drop in resistance from samples 8 and 11 to sample 9 in Figure 3.2.2 could very well indicate a transition from hopping to metallic like conduction.

In summary this thesis supports the existence of metallic like conduction within an impurity band of vacancy donor states over the temperature region of 90 to 300 K for heavily reduced samples of $Bi_3FeMo_2O_{12}$.

APPENDIX A

Mo O3
Molybdenum Oxide
Molybdite, syn
Hanawalt 3.26/X 3.81/8 3.46/4 6.92/4 3.44/3 2.65/3 2.31/2 2.70/2 1.85/2 2.27/1

Lambda 1.5405981
Sys. Orthorhombic
SG Pbnm PS oP 16.00
a 3.9630 b 13.856 c 3.6966
α β γ
A 0.2860 C 0.2668 Z 4
Dm Dx 4.710 V 202.99
F(N) 127.7 M(20) 170.1 I/Ic
d-sp Calculated spacings
Int Calculated intensities
Total d's 58
Color
Temp

d	Int	h	k	l	d	Int	h	k	l
6.921	36	0	2	0	2.332	8	1	3	1
3.808	77	1	1	0	2.308	21	0	6	0
3.463	38	0	4	0	2.270	13	1	5	0
3.439	31	1	2	0	2.131	7	1	4	1
3.259	100	0	2	1	1.995	2	1	6	0
3.007	7	1	3	0	1.981	8	2	0	0
2.702	15	1	0	1	1.958	12	0	6	1
2.652	26	1	1	1	1.934	1	1	5	1
2.607	3	1	4	0	1.905	1	2	2	0
2.526	7	0	4	1	1.848	15	0	0	2

Card 1, pattern 1 of 1

[Enter]=Next pattern, N=Next card, P=Previous card, B=Back :

delta - Bi2 O3
Bismuth Oxide

Hanawalt 3.27/X 1.71/7 2.00/7 2.83/5 1.30/3 1.27/2 1.63/2 1.16/2 0.96/2 1.09/2

Lambda 1.54434
Sys. Cubic
SG Fm3m PS cF 12.00
a 5.66 b c
α β γ

A 5.6600 C Z 2.4
Dm Dx V 181.32
F(N) 7.1 M(20) 24.3 I/Ic
d-sp Not given
Int Visual estimation from film
Total d's 12
Color
Temp Pattern at 750 C.

d	Int	h	k	l	d	Int	h	k	l
3.270	100	1	1	1	.9570	18	5	3	1
2.830	45	2	0	0	.9430	8	6	0	0
2.000	65	2	2	0					
1.710	70	3	1	1					
1.630	18	2	2	2					
1.420	10	4	0	0					
1.300	25	3	3	1					
1.270	20	4	2	0					
1.160	18	4	2	2					
1.090	16	5	1	1					

Card 1, pattern 1 of 1

[Enter]=Next pattern, N=Next card, P=Previous card, B=Back :

Bi
Bismuth
Bismuth, syn
Hanawalt 3.28/X 2.27/4 2.37/4 1.87/2 1.44/2 1.49/1 1.33/1 1.97/1 3.95/1 1.64/1

Lambda 1.5405
Sys. Rhombohedral
SG R-3m PS hR 2.00
a 4.546 b c 11.860
α β γ

A 2.6089 C Z 6
Dm 9.765 Dx 9.808 V 212.26
F(N) 47.1 M(20) 63.3 I/Ic
d-sp Not given
Int Diffractometer
Total d's 46
Color Grayish white
Temp X-ray pattern at 25 C.

d	Int	h	k	l	d	Int	h	k	l
3.950	9	0	0	3	1.639	9	0	2	4
3.740	3	1	0	1	1.556	6	1	0	7
3.280	100	0	1	2	1.515	2	2	0	5
2.370	40	1	0	4	1.491	13	1	1	6
2.273	41	1	1	0	1.443	16	1	2	2
2.030	8	0	1	5	1.387	4	0	1	8
1.976	3	0	0	6	1.330	11	2	1	4
1.970	10	1	1	3	1.319	1	0	0	9
1.941	1	0	2	1	1.312	6	3	0	0
1.868	23	2	0	2	1.284	2	0	2	7

Card 1, pattern 1 of 1
[Enter]=Next pattern, N=Next card, P=Previous card, B=Back :

Mo O2
Molybdenum Oxide
Tugarinovite, syn
Hanawalt 3.42/X 2.43/7 1.71/4 2.40/4 1.72/4 2.44/3 1.73/3 1.70/2 1.40/2 1.54/1

Lambda 1.540598
Sys. Monoclinic
SG P21/n PS mP 12.00
a 5.6068 b 4.8595 c 5.5373
α β 119.37 γ
A 1.1538 C 1.1395 Z 4
Dm Dx 6.463 V 131.48
F(N) 29.7 M(20) 39.6 I/Ic
d-sp Not given
Int Diffractometer
Total d's 39
Color Black
Temp Pattern taken at 25 C.

d	Int	h	k	l	d	Int	h	k	l
4.805	2	-1	0	1	1.841	11	-3	0	1
3.420	100	-1	1	1	1.725	30	2	1	1
2.813	4	1	0	1	1.723	35	-2	2	0
2.442	30	2	0	0	1.711	40	-3	1	2
2.437	30	1	1	1	1.709	35	-2	2	2
2.426	70	-2	1	1	1.697	20	-2	1	3
2.403	35	-2	0	2	1.603	1	-3	0	3
2.181	6	2	1	0	1.544	7	-3	1	0
2.171	2	0	2	1	1.536	13	0	3	1
2.156	5	-2	1	2	1.527	9	0	1	3

Card 1, pattern 1 of 1
[Enter]=Next pattern, N=Next card, P=Previous card, B=Back :

REFERENCES

1. C.S. Hung and S.R. Gleissman, *The Resistivity and Hall Effect of Germanium at Low Temperatures*, Physics Review **79** 726-727 (1950).

2. C.S. Hung, *Theory of Resistivity and Hall Effect at Very Low Temperatures*, Physics Review **79** 727-728 (1950).

3. N.F. Mott, *On the Transition to Metallic Conduction in Semiconductors*, Canadian Journal of Physics **34** 1356-1368 (1956).

4. Kyoju Kimoto and S. Roy Morrison, *Electron and Oxygen Exchange between Reactants and Bismuth Molybdate*, Zeitshcrift für Physikalische chemic Neue Folge, Bd. **108** 11-32 (1977).

5. S. Roy Morrison, *Electron Exchange Processes in Olefin Oxidation*, Journal of Catalysis, **34** 462-478 (1974).

6. D.A.G. Van Oeffelen, J.H.C. Van Hooff, and G.C.A. Schuit, *In Situ Measurements of the Electrical Conductivity of Bismuth Molybdate Catalysts in Operation for Oxidative Dehydrogenation of Butene*, Journal of Catalysis, **95** 84-100 (1985).

7. K.M. Sancier, A. Aoshima and H. Wise, *Charge Transfer During Redox of Bismuth Molybdate Catalysts*, Journal Of Catalysis, **34** 257-266 (1974).

8. I. Matsuura and G.C.A. Schuit, *Absorption, Equilibria and Rates of Reactions of Absorbed Compounds on Reduced and Oxidized Bi-Mo Catalysts*, Journal of Catalysis, **20** 19-39 (1971).

9. Peter A. Thornton and Vito J. Colangelo, *Fundamentals of Engineering Materials*, Prentice-Hall, Inc., Englewood Cliffs, New Jersey, 342-349 (1985).

10. N.B. Hannay, *Semiconductors*, Reinhold Publishing Corporation, New York, 16-17 (1959).

11. S.M. Sze, *Physics of Semiconductor Devices*, John Wiley and Sons Inc., New York, 25-28 (1969).

12. Charles Kittel, *Introduction to Solid State Physics*, John Wiley and Sons, Inc., New York, 200-205 (1986).

13. N.B. Hanney, *Semiconductors*, Reinhold Publications Corporation, New York, 24-34 (1959).

14. R.A. Greiner, *Semiconductor Devices and Applications*, McGraw-Hill Book Company Inc., New York, 58-72 (1961).

15. Neil W. Ashcroft and N. David Mermin, *Solid State Physics*, W.B. Saunders Company, 562 (1976).

16. Ibid, 578-579.

17. N. B. Hannay, *Semiconductors*, Reinhold Publications Corporation, New York, 17-24 (1959).

18. M.S. Tyagi, *Introduction to Semiconductor Materials and Devices*, John Wiley and Sons Inc., 69-73 (1991).

19. Peter A. Thornton and Vito J. Colangelo, *Fundamentals of Engineering Materials*, Prentice-Hall Inc., Englewood Cliffs, New Jersey, 349 (1985).

20. K. Seeger, *Semiconductor Physics*, Springer-Verlag and Wien, New York, (1973).

21. R.A. Grenier, Semiconductor Devices and Applications, McGraw-Hill Book Company Inc., New York, 65-72 (1961).

22. M.S.Tyagi, *Introduction to Semiconductor Materials and Devices*, John Wiley and Sons Inc., 105-107 (1991).

23. C.S. Hung and V.A. Johnson, *Resistivity of Semiconductors Containing Both Acceptors and Donors*, Phys. Rev. **79** 535-536 (1950).

24. Mott and Davis, *Electronic Processes in Non-Crystalline Materials*, Clarendon Press Oxford, 121 (1971).

25. C.S. Hung and J.R. Gliessman, *Resistivity and Hall Effect of Germanium at Low Temperatures*, Physical Review **96** 1226-1236 (1954).

26. N.F. Mott and W.D. Twose, *The Theory of Impurity Conduction*, Advances in Physics, **10** 107-163 (1961).

27. H. Fritzsche, *Resistivity and Hall Coefficient of Antimony Doped Germanium at Low Temperatures*, J. Phys. Chem. Solids **6** 69-80 (1958).

28. Mott and Davis, *Electronic Processes in Non-Crystalline Materials*, Clarendon Press Oxford, 152-156 (1971).

29. Ester M. Conwell, *Impurity Band Conduction in Germanium and Silicon*, Physical Review, **103** 51-61 (1956).

30. A.L. Efros, Nguyen Van Lien and B.I. Shklovskii, *Impurity band structure in lightly doped semiconductors*, J. Phys. C: Solid State Phys **12** 1869-1881 (1979).

31. B.I. Shklowskii, *Hopping Conduction in Heavily Doped Semiconductors*, Soviet Physics - Semiconductors **7**, 77-80 (1993).

32. B.I. Shklovskii, *Hopping Conduction in Lightly Doped Semiconductors (Review)*, Soviet Physics - Semiconductors **6** 1053-1075, (1973).

33. E.C. McIrvine, *Phenomenology of Impurity Conduction in Semiconductors*, J. Phys. Chem. Solids **15** 356-358 (1960).

34. S.M. Sze, *Physics of Semiconductor Devices*, John Wiley and Sons Inc., New York, 20 and 30 (1969).

35. E.L. Wolf and W.D. Compton, *Annealing of Newton Irradiation - Induced Changes in Impurity Conduction in Antimony-Doped Germanium*, Journal of the Physical Society of Japan, **21** 561-565 (1966).

36. P.P. Debye and E.M. Conwell, *Electrical Properties of n-type Germanium*, Physical Review, **93** 693-706 (1954).

37. F.J. Morin and J.P. Maita, *Electrical Properties of Silicon Containing Arsenic and Boron*, Physical Review, **96** 28-35 (1954).

38. G.L. Pearson and J. Bardeen, *Electrical Properties of Pure Silicon and Silicon Alloys Containing Boron and Phosphorus*, Physical Review **75** 865-883 (1949).

39. *Handbook of Chemistry and Physics*, 68 Edition, E.104 and E. 105 (1987-1988).

40. N.B. Hannay, *Semiconductors*, Reinhold Publishing Company Corporation, New York, 585 (1959).

41. S. Toyotomi and K. Morigaki, *Journal of the Physical Society of Japan*, **25** 807-815 (1968).

42. B.R. Sethi, P.C. Mathur and J. Woods, *Impurity Band Conduction in Compensated ZnSe Crystals*, J. Appl. Phys. **49** 3618-3620 (1978).

43. G. Jones and J. Woods, *The Electrical Properties of Zinc Selenide*, J. Phys. D: Appl. Phys., **9** 799-810 (1976).

44. P.J. Sebastian and V. Sivaramakrishnan, *The Change of Electrical Conduction in the Valence/Conduction Band to the Impurity band in $CdSe_xTi$-x Thin Films*, J. Appl. Phys., **67** 3536-3538 (1990).

45. A.P. Belyaev, I.P. Kalinkin, and V.A. Sanitarov, *Electrical Conductivity of Films of Solid Solutions Based on Cadmium Selenide and Telluride*, Sov. Phys. Semicond., **18** 1234-1239 (1984).

46. W.M. Sears, *The gas-sensing properties of sintered bismuth iron molybdate catalyst*, Sensors and Actuators, **19** 351-370 (1989).

47. L. David Krenzke and George W. Keulks, *The Catalytic Oxidation of Propylene*, Journal of Catalysis, **61** 316-325 (1980).

48. PH. A Batist, C.J. Kapteijns, B.C. Lippens and G.C.A. Schuit, *The Catalytic Oxidation of 1-Butene over Bismuth Molybdate Catalysts. III. The Reduction of Bismuth Oxide, Molybdenum Oxide, Bismuth Molybdate, and of some Nonstoichiometric Molybdenum Oxides with 1-Butene*, Journal of Catalysis, 7 33-49 (1967).

49. W.M. Sears, *Vacancy Induced Transition in the Conductance of Bismuth Iron Molybdate*, Semicond. Sci. Technol. 7 1464-1470 (1992).

50. A.W. Sleight and W. Jeitschko, *$Bi_3(FeO_4)(MoO_4)_2$ and $Bi_3(GaO_4)(MoO_4)_2$ - New Compounds with Scheelite Related Structures*, Mat. Res. Bull **9** 951-954 **(1974)**.

51. W. Jeitschko, A.W. Sleight, W.R. McClellan and J.F. Weiher, *A Comprehensive Study of Disordered and Ordered Scheelite-Related $Bi_3(FeO_4)(MoO_4)_2$*, Acta Cryst., **B32** 1163-1170 (1976).

52. Andrew Guthrie, *Vacuum Technology*, Robert E. Krieger Publishing Company, Malabar, Florida, (1990).

53. W.M. Sears, *Vacancy donors and the electrical properties of bismuth iron molybdate pellets*, Sensors and Actuators **B12** 95-102 (1993).

54. S. Roy Morrison, *Semiconductor gas sensors*, Sensors and Actuators, **2** pp. 329-341 (1982).

55. K.M. Sancier, T. Dozono and H. Wise, *ESR spectra of metal oxide catalyst during propylene oxidation*, J. Catal. **23** 270-280 (1971).

56. J.M. Peacock, *The Oxidation of Propene over Bismuth Oxide, Molybdenum Oxide and Bismuth Molybdate Catalyst*, Journal of Catalysis, **15** 387-397 (1969).

57. J.B. Goodenough, *Metallic Oxides*, Prog. Solid State Chem. **5** 359 (1971).